Advances in ship-based air-sea CO_2 flux measurement by eddy covariance

B. W. Blomquist[1,3], L. Bariteau[3], J. W. Edson[2], C. W. Fairall[3], J. E. Hare[4],W. R. McGillis[5] B. J. Huebert[1], S. D. Miller[6], E. S. Saltzman[7]

Corresponding author: B.W. Blomquist, Department of Oceanography, University of Hawaii, 1000 Pope Rd., Honolulu, HI 96822, USA. (blomquis@hawaii.edu)

[1]Department of Oceanography, University

Abstract. [Abstract to be determined, pending revisions and additions.]

of Hawaii, Honolulu, Hawaii, USA.

[2]Department of Marine Sciences, University of Connecticut, Groton, Connecticut, USA.

[3]Earth System Research Laboratory, NOAA, Boulder, Colorado, USA.

[4]Joint Institute for Marine and Atmospheric Research, University of Hawaii, Honolulu, Hawaii, USA.

[5]Lamont Doherty Earth Observatory, Columbia University, Palisades, New York, USA.

[6]Atmospheric Sciences Research Center, State University of New York at Albany, Albany, New York, USA.

[7]Earth System Science, University of California, Irvine, California, USA.

1. Introduction

Eddy covariance (EC) is a well established surface flux technique in carbon cycle research. Continuous flux observations are now routine across a global network of land-based sites [http://fluxnet.ornl.gov, *Baldocchi et al.*, 2001], largely directed at determining net ecosystem exchange (NEE) over seasonal timescales. The terrestrial research community has a clear focus on flux bias issues which may integrate to large errors in NEE, and a general consensus exists concerning standardized methods and data analysis procedures [e.g. *Lee et al.*, 2004].

In contrast, the objectives of marine CO_2 EC flux measurements are focused on short timescales of 15 minutes to 1 hour, where the the effects of physical forcing factors may be examined. The principal motivation for air-sea flux measurements is development and validation of bulk flux and empirical gas transfer models for prognostic analysis of the ocean's role in energy budgets and biogeochemical cycles. The oceans are a net sink for carbon dioxide – roughly $2\,\mathrm{Pg\,C\,yr^{-1}}$ or one-third of the estimated annual anthropogenic production of CO_2 [*Takahashi et al.*, 2002; *Sabine et al.*, 2004; *Jacobson et al.*, 2007; *Takahashi et al.*, 2009]. Global carbon cycle models are well developed, and in these models the air-sea CO_2 transfer coefficient, k_{co_2}, is often simulated by polynomial functions of the mean 10-meter wind speed ($\overline{u}_{10}$). A variety of quadratic and cubic wind speed dependencies have been proposed [e.g. *Wanninkhof*, 1992; *Nightingale et al.*, 2000; *Ho et al.*, 2006; *Sweeney et al.*, 2007; *Wanninkhof and McGillis*, 1999; *McGillis et al.*, 2001a; *Prytherch et al.*, 2010a; *Edson et al.*, 2011]. In a study comparing the effects of quadratic and cubic representations, *Takahashi et al.* [2002] found a 70 % enhancement in both

annual CO_2 uptake and wind speed sensitivity for the cubic k_{co_2} model. An uncertainty this large lends urgency to the task of identifying and quantifying the factors controlling air-sea gas exchange.

Contrasting experimental approaches for air-sea gas transfer studies have been developed: tracer studies utilizing ambient gases (Rn, $^{14}CO_2$) or deliberately introduced tracers (He, SF_6) which integrate flux over timescales of a week or more [e.g. *Wanninkhof*, 1992; *Nightingale et al.*, 2000; *Ho et al.*, 2006; *Sweeney et al.*, 2007; *Ho et al.*, 2011], and direct EC flux measurements of CO_2 on hourly timescales [e.g. *McGillis et al.*, 2001a, 2004; *Kondo and Tsukamoto*, 2007; *Weiss et al.*, 2007; *Prytherch et al.*, 2010a; *Miller et al.*, 2009, 2010; *Lauvset et al.*, 2011; *Edson et al.*, 2011]. In general, EC measurements tend to support a cubic wind speed dependence for k_{co_2} while results from tracer studies appear quadratic, although one long-term EC study at an inland-sea site with limited wind fetch also seems consistent with a quadratic model [*Weiss et al.*, 2007]. Solubility differences are surely one source of variability in k among the various gases, but a full explanation of the discrepancies remains elusive. There are large uncertainties associated with both experimental approaches. Improving EC measurement precision is therefore a high priority.

While the principles of EC flux measurements on land and sea are the same, marine studies present several unique problems. The oceanography community has yet to reach a consensus on methods to deal with all of these issues. Except in shallow coastal areas where fixed platforms are feasible, measurements must be made from a ship or moored buoy. Motion induced by waves and by changes in ship heading prevent a fixed coordinate frame of reference; high-rate wind measurements must therefore be corrected for platform

tilt, rotation, and velocity. Inevitable air-flow distortion caused by the ship's superstructure should be minimized and mean wind speeds corrected for its effects. Equipment must function in a hostile environment of salt spray and sooty emissions, where opportunities for cleaning and servicing in-situ sensors are often limited by hazardous conditions. Perhaps most important, air-sea CO_2 fluxes are quite small, often less than 3 mmol m^{-2} d^{-1} (1.5×10^{-3} mg CO_2 m^2 s^{-1}), yielding a concentration variance of at most few tenths of a ppm on a background concentration of ∼390 ppm. A small flux over the vast expanse of the ocean is nevertheless significant to the global carbon cycle. This places a premium on adequate signal-to-noise performance and freedom from interferences.

Marine CO_2 flux measurements have been done for at least 15 years. Several studies reporting ship-based EC measurements of CO_2 flux are listed in Table 1. Flux measurements with closed-path infrared gas analyzers (CP-IRGA) on early cruises (e.g. GasEx-98 and -01) were largely successful, despite numerous measurement challenges. There are well known issues related to EC sampling uncertainty, flow distortion, spectral attenuation, and density effects (i.e. the Webb, Pearman, Leuning or WPL theory: *Lee and Massman* [2011]; *Webb et al.* [1980]), many of which can be corrected during data processing or minimized by appropriate experimental design. However, the early trials revealed an additional interference related to platform motion. Water vapor cross-sensitivity, inherent to the broadband IR method, contributes further uncertainty [*Fairall et al.*, 2000; *McGillis et al.*, 2001a]. In general, the detection limit was insufficient to observe fluxes over much of the ocean surface, limiting gas exchange studies to areas where air-sea CO_2 disequilibruim is large ($|\Delta pCO_2| > 80$ ppm).

Subsequent studies tended to prefer the open-path gas analyzer configuration (OP-IRGA) due to inherent advantages in frequency response, power consumption and wind measurement synchronization. To-date, the popular choice has been a commercial instrument commonly used in terrestrial flux studies, the LI7500 (LI-COR Biosciences, Lincoln, Nebraska, USA). Unfortunately, experience has shown the effects of optical contamination and water vapor cross-sensitivity are severe with this design and complex corrections are required [*Kohsiek*, 2000; *Prytherch et al.*, 2010b; *Edson et al.*, 2011]. Much of the discrepancy between observed and expected flux reported by *Kondo and Tsukamoto* [2007] may stem from this interference. As a result, flux measurement accuracy and precision has not improved. A case can be made that early CP-IRGA measurements were superior, although *Prytherch et al.* [2010b] and *Edson et al.* [2011] demonstrate some success in correcting the OP-IRGA water cross-sensitivity in post-processing. Corrections, however, are an order of magnitude larger than the flux.

Miller et al. [2010] have used an OP-IRGA in a modified closed-path configuration with promising results. A smaller, weather-proof version of the CP-IRGA with a very short sample inlet tube is now available (LI-COR model LI7200), as are fast, high-sensitivity closed-path trace gas analyzers based on cavity-enhanced IR absorption and cavity ring-down spectrometry. Clearly, technology is advancing and new instruments are gaining wide acceptance in the carbon cycle research community. Their eventual use on ship platforms is inevitable.

It is appropriate at this time to summarize what has been learned over the last decade of ship-based CO_2 flux studies, examine the latest technical innovations, and begin the discussion toward a set of recommended experimental and data analysis procedures for

EC flux measurements at sea. Our objectives in this paper are to: 1) present a summary review of the instrumental methods available, including principle interferences and advantages of each; 2) examine the relative performance of new analyzers with respect to the established methods, and; 3) discuss the most significant errors resulting from instrumental and meteorological causes and show how they may be eliminated, minimized or at least identified and removed from the data set. Flux data from two recent field programs will be used as a basis for critical evaluation of new methods. We conclude with a set of recommendations which seem to offer the best flux measurement precision under typical conditions for ship-based deployments.

2. Overview of Instrumental Methods

In this section we focus on a brief description of CO_2/H_2O analyzers suitable for flux measurements at sea, including their inherent advantages and disadvantages. Specific approaches to overcome interferences will be discussed in Section 6. All EC flux measurements require a fast, 3-axis wind measurement and sonic anemometers are the established standard. Several models are commercially available and most have performed well on ships. We will not consider the wind measurement system in this report except to review motion correction issues in Section 6.

2.1. Broadband IR Absorption Gas Analyzers

Closed-path IRGA instruments were the first to be developed and deployed for EC flux measurements [e.g. *Jones et al.*, 1978] and commercial versions have been available for many years (e.g. LI-COR models LI6262, LI7000 and more recently the LI7200). All of these measure H_2O simultaneously with CO_2. A broadband light source is used

with a chopper–filter wheel to sequentially measure infrared absorption at narrow bands corresponding to CO_2, H_2O and low-absorbance background regions of the spectrum. Compensation for zero-drift and cross-sensitivity (memory effects) in the IR detector are necessary, and a band-broadening correction is computed for CO_2 based on the measured H_2O mole fraction (see LI7500 CO2/H2O Analyzer Instruction Manual, Section 2 and LI-COR Application Note 129). Newer versions of the CP-IRGA measure optical cell temperature and pressure, enabling a real-time computation of molar mixing ratio from the measured molar density concentration.

Except for the LI7200, CP-IRGA are bench-scale laboratory instruments and must be located in a protected environment. The obvious disadvantages are frequency attenuation in sample line tubing (low pass filtering) and a time lag between the wind and gas concentration measurements. In principle, both of these problems can be addressed by appropriate experimental design. For example, maintaining a high flow rate in the sample line greatly reduces signal attenuation [*Lenschow and Raupach*, 1991] and correction procedures for spectral attenuation have been developed and tested [e.g. *Moore*, 1986; *Massman and Lee*, 2002; *Lee et al.*, 2004; *Ammann et al.*, 2006]. Signal lag may be measured precisely with a timed pulse of nitrogen or zero air at the sample inlet (e.g. one 3 second pulse per hour), inducing a spike in the CP-IRGA response which is matched to the digital trigger pulse recorded on the wind data system [as in *Bariteau et al.*, 2010].

An open-path IRGA employs the same operational principles in a miniaturized, weatherproof form suited to installation on sampling towers for in-situ measurements. Several early designs were developed [*Ohtaki and Matsui*, 1982; *Kohsiek*, 1991; *Auble and Meyers*, 1992] but the LI-COR LI7500 is the OP-IRGA in widespread use at this time. The

open-path design achieves superior frequency response and close synchronization with sonic wind measurements. The sensor body presents a wind obstruction and must be located an appropriate distance from the anemometer ($\sim$1 m). At the height where ship measurements are typically made, 15 m to 20 m above the surface, this degree of sensor separation should not result in significant loss of correlation. Lacking a sample pump, power consumption is very low, which is an advantage in situations with limited power (i.e. buoys or near-shore towers). However, with an open-path optical cell it is not possible to measure temperature and pressure in the sample volume with sufficient speed and accuracy for a high-precision computation of molar mixing ratio. Open-path IRGA CO_2 concentrations are typically computed as molar or mass density with appropriate WPL corrections applied as necessary.

Motion-related interference is a problem for all IRGA analyzers at sea. The root causes of motion sensitivity are unclear. Interference with the chopper wheel [*McGillis et al.*, 2001a] and flexing of the source filament [*Miller et al.*, 2010] have both been proposed. *Miller et al.* [2010] also identify a hydrostatic pressure perturbation related to vertical heave. Any of these may correlate with residual motion contamination in the vertical wind measurement, leading to error in the computed flux.

Water vapor interference is perhaps the most significant problem. In theory, the LI-COR algorithm accounts for band-broadening and cross-sensitivity. The correction is not perfect, however, and for a situation of minuscule CO_2 flux in the presence of a large H_2O flux, imprecision inevitably leads to bias in the computed CO_2 concentration. For the open-path instrument, water vapor effects are exacerbated by the accumulation of salt, sea spray and grime on the optics. Additional signal variance from any of these

interferences may exceed variance from the true CO_2 surface flux. Because the interference may correlate with water vapor flux (and vertical wind), the resulting CO_2 cospectrum is often dominated by water vapor crosstalk, leading to as much as a factor of ten error in the computed CO_2 flux. Corrections for this interference are possible [*Prytherch et al.*, 2010b; *Edson et al.*, 2011], but measurement precision is inevitably degraded.

2.2. Cavity-Enhanced IR Absorption and Cavity Ring-Down Spectrometers

Over the past two decades, advances in continuous-wave tunable diode laser (CW-TDL) technology have led to the development of several promising methods suitable for trace gas flux studies at ppm and ppb levels. At a reduced pressure ($\sim 18\,\mathrm{kPa}$), small gas molecules such as CO_2, H_2O, N_2O and CH_4 exhibit complex IR and near-IR spectra with a host of unique, narrow absorption lines ($\Delta\nu_{fwhm} \sim 0.05\,\mathrm{cm}^{-1}$). The height or area of a peak in the absorption spectrum is proportional to the absorbing molecule's molar density through Beer's Law, which may be further adjusted to a dry gas basis if H_2O is measured simultaneously. Because cavity temperature and pressure are carefully controlled, molar mixing ratios are easily computed. Furthermore, because absorption lines are unique not only to a chemical species but to a particular isotopomer of each species, these methods may be applied to isotopic flux studies [*Griffis et al.*, 2008]. Sensitivity is achieved by selecting a strong absorption line and employing a very long path (tens of km) "cavity-enhanced" optical cell. Frequency response is $\geq 2\,\mathrm{Hz}$, limited primarily by flow rate and cavity volume. Two variants of the method are commercially available at this time.

Cavity ring-down spectrometers (CRDS) were first developed more than 20 years ago [*O'Keefe and Deacon*, 1988]. Following a pulse of light into an evacuated optical cavity, detector response is seen to decay with a time constant dependent on mirror reflectivity.

Higher reflectivity leads to longer characteristic decay time and path length. 99.999 % reflectance and 10 km to 20 km path lengths are typical. The incremental reduction in decay time when absorbing molecules are introduced is proportional to absorbance. Decay time measurements at a series of discrete wavelengths across an absorption line (7-9 points) define the absorption peak, and a Voigt function fit to these points determines peak height, which is proportional to gas concentration. Because line shape is a function of temperature and pressure in the optical cell, these conditions must be controlled to very high tolerances – pressure to one part in a thousand and temperature to $\pm 0.02\,^{\circ}$C. TDL wavelength is controlled to a precision of about one-thousandth of the line width. The optical cell must be manufactured to exceedingly close tolerances and is quite sensitive to contamination, requiring a particle pre-filter. TDL bandwidth is limited to a few wavenumbers at most, so the laser source is manufactured to suit each specific application and multi-gas analyzers often require multiple lasers. CRDS analyzers for a variety of trace gases and analytical applications are commercially available (Picarro Inc., Santa Clara, California, USA).

A similar method based on direct absorbance has been recently developed [*O'Keefe et al.*, 1999; *Baer et al.*, 2002]. Off-axis integrated cavity output spectroscopy (OA-ICOS) employs a cavity-enhanced optical cell of similarly long effective path length. The TDL source scans continuously across the absorbance lines to record the spectrum. Tolerances for cell construction, temperature/pressure control, and source wavelength tuning control are somewhat relaxed in this method. Wavelengths in the near-IR, not generally useable with CRDS, are feasible with OA-ICOS. Concentrations are computed by fitting a Voigt line shape function to the spectral peaks. Because the laser is tuned across the entire absorbance peak, more information is available for the fit and overlapping lines may be

resolved with a multi-component fit. Absorbances are easily calibrated to yield mole fraction on a moist and dry basis. As with CRDS, OA-ICOS analyzers for a variety of gases are available (Los Gatos Research, Mountain View, California, USA).

With cavity-enhanced methods, pressure broadening of the absorption line leads to cross-sensitivity with other components in the gas mixture. Water vapor is once again the principal offender. A correction for line broadening is therefore necessary, and most analyzers include a water measurement in addition to the specific gases of interest. Because these are bench-scale instruments requiring sample inlet tubes, the usual caveats with respect to time lag and spectral attenuation also apply.

3. Experimental

CO_2 flux measurements were included on two recent field programs as part of an ongoing effort to develop and evaluate new methods. Full results for these cruises are not yet available but an analysis of flux measurements is complete. In this section we present a brief overview of the experimental conditions and cruise details relevant to the flux tests.

3.1. DYNAMO

Project CINDY2011/DYNAMO (Cooperative Indian Ocean Experiment on Intraseasonal Variability in Year 2011 / Dynamics of the Madden-Julian Oscillation) was a multinational, multi-platform investigation of ocean-atmosphere interaction in the Equatorial Indian Ocean. As one of three platforms providing DYNAMO surface observations, the ship R/V Roger Revelle occupied a station near 0°N, 80°E for the period August 2011 to February 2012, with periodic transits to Phuket, Thailand for resupply (see Figure 1). In this report we focus on Leg 3, from 07-Nov to 08-Dec-2011.

The NOAA/ESRL portable flux system [*Fairall et al.*, 1997, 2003] on the R/V Revelle recorded 10 Hz wind and motion measurements, bulk meteorological variables and sea surface temperature (SST). Three CO_2 IRGA analyzers were installed in the following configurations: two LI7500 OP-IRGAs and one LI7200 CP-IRGA (University of Connecticut), mounted near the wind and motion sensors on the ship's forward mast; and one LI7200 (NOAA/ESRL) installed in a shipping container lab on the deck, drawing air from a teflon sampling tube extending up to the location of the mast flux sensors (30 m, 0.95 cm ID). Because the LI7200 differential pressure sensor has limited range, pressure drop considerations restricted inlet line flow to $<40\,\mathrm{L\,min^{-1}}$ STP for the lab analyzer. Optics for the LI7500 OP-IRGA were rinsed daily with distilled water to limit the effects of surface contamination.

A 200-tube Nafion air dryer (PD-200T-24-SS, Perma Pure LLC, Toms River, New Jersey, USA) was used with the lab analyzer to reduce sample air dew point to $<-10\,^{\circ}\mathrm{C}$; water vapor band-broadening and dilution corrections for the lab LI7200 analyzer were therefore insignificant. The mast mounted LI7200 flow rate was $17\,\mathrm{L\,min^{-1}}$ through a 1 m by 0.95 cm ID inlet tube; the lab-mounted LI7200 analyzer subsampled the high-flow inlet at $\sim 4\,\mathrm{L\,min^{-1}}$ STP and a pressure of $\sim$940 mb. Both LI7200 analyzers record high-rate cell temperature and pressure for automated computation of dry CO_2 mole fraction.

A small equilibrator system and LI-COR 840 CO_2/H_2O analyzer from Lamont-Doherty Earth Observatory was used to measure air-sea ΔpCO_2 from the ship's clean seawater supply. Measurements alternated between the atmospheric and equilibrator gas samples. A Nafion air dryer was used on the LI840 sample stream ($0.8\,\mathrm{L\,min^{-1}}$) to obtain dry-air concentrations.

Fluxes from the three IRGA analyzers were computed from the standard "dry" mole fraction output of the LI7200 and the raw molar density output of the LI7500, with the latter corrected for dilution and WPL density perturbations using a combination of fast and slow temperature and humidity measurements and for vertical heave hydrostatic effects as in *Edson et al.* [2011] (see Section 6.1). Cospectra were computed from linearly detrended, motion corrected vertical wind velocity and fast CO_2 fluctuations in 10-minute segments. Filtering criteria for relative wind direction, ship maneuver parameters and reasonable limits on other variables such as motion correction variances were applied to remove questionable measurement conditions: specifically, relative wind within 90° of the bow, σ(heading) less than 5° and σ(ship velocity) less than $1\,\mathrm{m\,s^{-1}}$. In addition, limits on $\partial CO_2/\partial t$, $\overline{u'co_2'}$ and $\overline{v'co_2'}$ were used to select for steady-state CO_2 conditions (see discussion in Section 6.7).

3.2. TORERO

Project TORERO (Tropical Ocean Troposphere Exchange of Reactive Halogen Species and Oxygenated VOC) was a multi-platform field program focussing on the distribution, reactivity and abundance of oxygenated organics and halogen radicals over the Eastern Pacific, from Costa Rica south to Chile. Surface observations on the NOAA ship R/V Ka'imimoana were performed from 10°N to 10°S along the 110°W and 95°W TAO buoy lines. The cruise covered the period 25-Jan-2012 to 27-Feb-2012, including transit from Honolulu, Hawaii at the start and to Costa Rica at the conclusion (see Figure 1).

A flux instrument package of wind and motion measurements equivalent to the DYNAMO system was installed on the R/V Ka'imimoana. Sensors were mounted at the top of a 10-meter meteorological tower on the ship's bow. Data acquisition hardware

and a CRDS fast CO_2 analyzer (Picarro model G1301) were located in the ship's instrumentation lab, ∼40 m aft of the bow tower. Compared to DYNAMO, gas sample inlet tubing was longer with more than double the flow: ∼60 m, 0.95 cm ID, and 80 L min^{-1} STP. Air pressure was ∼700 mb at the analyzer inlet. Flow into the analyzer was controlled at ∼5 L min^{-1} STP and, as in DYNAMO, an identical Nafion air dryer removed water vapor from the CO_2 sample stream. The CRDS analyzer differs in one respect from a standard G1301 design with dual H_2O and CO_2 measurements; this spectrometer is configured to omit H_2O, devoting all measurement cycles to CO_2, yielding somewhat improved signal-to-noise performance (typically $\sigma_{co2} < 0.10$ ppm at 10 Hz).

Wind measurements (10 Hz) were corrected for motion interference using the *Edson et al.* [1998] method, with additional procedures as discussed in Section 6.5. Flux results were processed in 30-minute data segments with 10-minute overlap (i.e. four 30-minute segments per hour). The linear trend was subtracted from each data segment and a Hamming window applied to limit leakage of low frequency drift. Flux results were filtered with basic wind criteria: relative wind direction within 60° of the bow and standard deviation in relative wind direction <10° per 30-minute segment. Additional stationarity criteria and corrections for CRDS motion interference are discussed in sections 6.7 and 6.3 respectively.

4. Results: Flux Observations

4.1. DYNAMO

During DYNAMO, wind conditions were light and variable, punctuated by periodic wind events when the active phase of the Madden-Julian Oscillation (MJO) was observed, starting on 24-Nov (Figure 2, upper panel). The atmospheric CO_2 concentration remained

constant at ∼395 ppm with slight increases on 11-Nov and 23-Nov (Figure 2, lower panel). Leg 3 ΔpCO_2 was 20 ppm to 30 ppm, indicative of a weak source region for CO_2 (Figure 2, middle panel).

Because ΔpCO_2 for Leg 3 was positive and small, conditions were near the flux detection limit of the IRGA instruments, especially when winds were light. Throughout Leg 3 we expect a small, positive CO_2 flux. Figure 3 shows flux observed by the lab LI7200 is near zero or slightly positive, which confirms these expectations. This analyzer shows a clear increase in CO_2 flux during strong winds on Nov 23-24 and Nov 28-29. In contrast, results from the mast LI7200 in the upper panel of Figure 3 show a much larger positive CO_2 flux, highly correlated to the water vapor flux ($\overline{w'q'}$, blue trace). The mast LI7500 sees a large negative CO_2 flux, anti-correlated to $\overline{w'q'}$. Mast measurements in Figure 3 incorporate WPL and dilution adjustments, and all IRGA CO_2 measurements include an internal LI-COR correction for water vapor crosstalk. Clearly, additional water vapor corrections are necessary for mast-mounted analyzers. Fluxes corrected with a cross-correlation procedure are shown in Figure 3 lower panel and discussed in Section 6.2.

A correlation between CO_2 mole fraction and air conditioner cycling was noted for the lab-mounted LI7200. Although this analyzer is temperature compensated, we observe a clear residual sensitivity to ambient temperature fluctuations. Both analyzer and sample line were insulated to damp this artifact. The AC cycling frequency was sufficiently low that concentration drift related to room temperature variability should not contribute to flux over 10-minute integration times.

4.2. TORERO

The TORERO cruise track transited a weak CO_2 sink region SE of Hawaii, eventually crossing a sharp boundary near the equator into the East Pacific cold-tongue upwelling, a persistent feature in pCO_2 climatology characterized by $\Delta pCO_2 > 100\,\mathrm{ppm}$ [*Takahashi et al.*, 2009] (see Figure 1). Wind speeds were in excess of $10\,\mathrm{m\,s^{-1}}$ during the transit from Hawaii, but slackened considerably near the equator and into the cold-tongue region.

CO_2 flux, wind speed and sea surface temperature are summarized in Figure 4. Seawater CO_2 measurements are not available for this cruise, but on the basis of January-February ΔpCO_2 climatology in Figure 1 we expect the initial portion of the transit from Hawaii to be a weak sink region, with $\Delta pCO_2 \sim -20\,\mathrm{ppm}$ to $-30\,\mathrm{ppm}$. The cold tongue region south of the equator should be a strong CO_2 source. Flux observations in Figure 4 confirm these expectations. The flux detection limit of the CRDS system is more than sufficient to reveal a negative flux across the weak sink region early in the cruise.

Estimating air-sea disequilibrium from the observed CO_2 flux is an interesting exercise which serves as a sanity check on the quality of flux measurements. In Figure 5, ΔpCO_2 computed from the CRDS flux data and bulk flux model estimates of the transfer coefficient [k_{co2} from COAREG 3.0, *Fairall et al.*, 2011] compares favorably with January-February mean ΔpCO_2 from equatorial cruise data in the region from 95°W to 110°W [gridded SOCAT database: http://www.socat.info, *Sabine et al.*, 2012]. Trends in estimated TORERO ΔpCO_2 closely track the multi-year mean latitude gradient for this region.

5. Results: CO_2 Analyzer Performance

5.1. Noise Characteristics

Variance spectra for the CO_2 analyzers are presented in Figure 6. CRDS background noise is "pink" with a characteristic slope of $\sim -1/2$. There is some indication of turbulent variance following a $-5/3$ power law at low frequencies in the mean TORERO spectrum which may be due to turbulent diffusion of horizontal atmospheric concentration gradients, but signal variance is largely dominated by sensor noise. CRDS noise (1σ) over the flux bandpass of 0.001 Hz to 5 Hz is 0.07 ppm.

Background noise in the IRGA analyzers may also be "pink" based on the lab test spectrum for the LI7200 at constant CO_2 concentration, which is comparable to the CRDS result. However, LI7200 spectra have an unexplained hump at 0.3 Hz to 0.6 Hz which is unrelated to water or motion interference and may arise from internal processing of the raw absorbances. This feature is not apparent in cospectra and therefore may not propagate into the flux measurement. A considerable fraction of IRGA CO_2 signal variance in moist air is due to water vapor crosstalk, illustrated by spectra of cross-correlation corrected CO_2 data (Figure 6, dashed lines).

5.2. Flux Detection Limit

To investigate the flux detection limit, we examine theoretical flux error as a function of air-sea disequilibrium (ΔpCO_2) and wind speed ($\overline{u}$). Flux error may be specified as a function of variance in both vertical wind (w) and scalar (CO_2) measurements, where CO_2 variance is composed of an atmospheric vertical turbulent flux component ($\sigma^2_{co_2\,a}$) and an "other noise variance" component ($\sigma^2_{co_2\,n}$, arising from analyzer noise, water vapor crosstalk and other interferences), and where T is sampling time in seconds [after *Fairall*

et al., 2000].

$$\delta F_{co_2} = \frac{2\,\sigma_w}{\sqrt{T}} \left[\sigma^2_{co_2\,a} \tau_{w\,co_2} + \sigma^2_{co_2\,n} \tau_{co_2\,n} \right]^{1/2} \tag{1}$$

The two terms in (1) are assumed to be independent, with characteristic integral time scales (τ). From the scatter in flux measurements under conditions where $\Delta p\mathrm{CO}_2$ is very low, and therefore $\sigma^2_{co_2\,a}$ is approximately zero, we can solve (1) for an empirical estimate of the "other noise" term.

$$\epsilon_n \equiv \sigma^2_{co_2\,n} \tau_{co_2\,n} \approx \left[\frac{\delta F^2_{co_2,0}\, T}{4\,\sigma^2_w} \right]_{\sigma^2_{co_2\,a} \approx 0} \tag{2}$$

Quantities σ_w, $\sigma^2_{co_2\,a}$ and $\tau_{w\,co_2}$ in (1) are stability dependent. Monin-Obhukov similarity scaling may be used to express the stability dependence of variances through the following relationships, where L is the Obukhov length in meters and u_* is the friction velocity. In addition, an empirical relationship (5) may be used to specify the integral time scale, where $b = 2.8$ is a constant, and the functions f_w, f_{co_2} and f_τ are similarity relationships specifying stability dependence (unity for neutral conditions) [see *Blomquist et al.*, 2010].

$$\sigma_w = 1.25\, u_* f_w(z/L) \tag{3}$$

$$\sigma_{co_2\,a} = \frac{3\,F_{co_2}}{u_*}\, f_c(z/L) \tag{4}$$

$$\tau_{w\,co_2} = b\,\frac{z}{\overline{u_r}}\, f_\tau(z/L) \tag{5}$$

$$f_w(z/L) = (1 + 3\,|z/L|)^{1/3} \qquad z/L < 0 \tag{6a}$$

$$f_w(z/L) = 1 + 0.2\,z/L \qquad z/L > 0 \tag{6b}$$

$$f_{co_2}(z/L) = (1 + 20\,|z/L|)^{-1/3} \qquad z/L < 0 \tag{7a}$$

$$f_{co_2}(z/L) = 1 + 1.0\,(z/L)^{1/2} \qquad z/L > 0 \tag{7b}$$

$$f_\tau(z/L) = [\min(5,\, \max(0.5,\, (1 + 0.6z/L))]^{-1} \tag{8}$$

Substitution of (3–8) into (1) yields an expression for flux error as a function of $\overline{u}$ and u_*, which can be further extended to the detection limit criterion, $\Delta p\mathrm{CO}_2(u)$, by assuming an arbitrary error condition (e.g. $\delta F/F = 1$, or 100% error), integration time (3600 seconds) and substitution of the standard bulk flux formulation, $F_{co_2}(u) = \alpha k(u)\Delta p\mathrm{CO}_2$.

$$\Delta pCO_2 = \frac{2.50\,u_*\,f_w}{\alpha\,k\,\sqrt{3600}}\left[\left(\frac{3\,F_{co_2}\,f_{co_2}}{u_*}\right)^2\,\frac{2.8\,z\,f_\tau}{\overline{u_r}} + \epsilon_n\right]^{1/2} \tag{9}$$

Here, $\overline{u}_r$ is mean relative wind speed (equivalent to $\overline{u}$ if the ship is not moving), α is dimensionless CO_2 solubility and k is the gas transfer coefficient. For this exercise, k, u_*, α and L were computed from the COAREG 3.0 bulk flux model [*Fairall et al.*, 2011, and references therein] with air temperature = 19 °C, SST = 20 °C, wind speeds from 1–16 $\mathrm{m\,s^{-1}}$ and default values for other inputs. For the various analyzers, empirical values for the "other noise" term in (2) were determined for periods of near-zero CO_2 flux, yielding the following values (all as ppm^2 s): $\epsilon_{n,CRDS} = 0.00057$, $\epsilon_{n,7500} = 0.04574$, $\epsilon_{n,7200(dry,lab)} = 0.00867$ and $\epsilon_{n,7200(mast)} = 0.02043$. These values assume the best possible correction for water vapor interference in the mast-mounted sensors (see Section 6.2). We assume that ϵ is a constant, but for analyzers with significant water vapor crosstalk the fraction of noise from that source may in fact have a wind speed dependence. Note that in (9), F_{co_2} is dependent on $\Delta p\mathrm{CO}_2$ and $\overline{u}$, so an iterative solution is necessary.

The detection limit criterion $\Delta pCO_2(u)$ computed from (9) for each analyzer is shown in Figure 7. The curves represent a theoretical lower limit on ΔpCO_2 for 100% error under slightly unstable, stationary conditions. $\Delta pCO_2(u)$ for error conditions other than $\delta F/F = 1$ scales inversely; for an error of $\delta F/F = 0.25$, the ΔpCO_2 criterion will be four times greater than indicated in Figure 7. We also note that, other things being equal, as SST decreases so does ambient ΔpCO_2 and therefore flux error will increase. From Figure 7 it is clear the analyzers with a dryer perform considerably better than those without. This is also generally apparent in the scatter of flux measurements from Figures 3 and 4. The estimated detection limit for the dry-air CRDS measurement represents a factor of 10 improvement over the earliest measurements with CP-IRGAs.

Figure 8 illustrates the CRDS detection limit as a function of the stability parameter z/L. In this case, k, L and u_* are obtained from COAREG model runs at two wind speeds ($u = 3$ and $8\,\mathrm{m\,s^{-1}}$) under conditions where all bulk variables other than air temperature are held constant (T_{air} = 8–16°C, SST = 12 °C, RH = 80% and all other variables at default values). At a moderate wind speed of $8\,\mathrm{m\,s^{-1}}$, the computed ΔpCO_2 criterion remains acceptable and the stability parameter has a narrow range about zero, even for large air-sea temperature gradients of ±4 °C. In light winds, however, z/L varies over a much wider range and flux measurements quickly become untenable under stable conditions when $z/L > 0.5$, or in this case when air temperature exceeds SST by ∼0.5 °C.

6. Results: Interferences and Corrections

Instrumental limitations, interferences, experimental constraints and meteorological conditions may all contribute to bias error in EC flux estimates. It is almost always necessary to apply corrections to computed cospectra or covariances to minimize these

errors, usually at the expense of a (hopefully small) increase in random error. In this section we discuss the most significant sources of bias error and examine methods to avoid or correct for their effects.

6.1. Density Perturbations

Corrections to molar density fluxes for perturbations caused by heat and pressure fluxes are a well known issue with EC measurements [see review of WPL theory by *Lee and Massman*, 2011]. For measurements on ships, *Miller et al.* [2010] have identified an additional pressure/density perturbation resulting from vertical heave. Other dynamic pressure effects are usually minor but may be important at higher wind speeds [*Zhang et al.*, 2011]. The sum of these interferences, if uncorrected, can lead to measurement bias greater than the actual ocean-atmosphere CO_2 flux. The OP-IRGA measurement is most affected by density fluctuations, requiring an accurate simultaneous determination of pressure fluctuations and sensible and latent heat fluxes. For the CP-IRGA, thermalization in a long sample line eliminates the need for a sensible heat flux correction. Dynamic pressure effects are probably also less significant, but a fast pressure measurement may nevertheless be required for heave-related corrections unless analyzer cell pressure is controlled to a constant value.

The fundamental assumption of WPL theory is a zero surface flux of dry air [*Webb et al.*, 1980]. The dry-air molar mixing ratio of a trace gas is a scalar quantity conserved in vertical motions and is therefore the preferred representation of concentration in conservation equations [*Kowalski and Argueso*, 2011]. It is a considerable advantage if the analyzer computes dry-air mixing ratio in real time from simultaneous measurements of CO_2, T, P and H_2O, eliminating the need for WPL corrections [*Nakai et al.*, 2011].

However, the accuracy of computed dry mole fraction is limited by calibration error and background noise in the T, P and H_2O measurements. Other things being equal, we expect the cavity-enhanced closed-path analyzers, which control the optical cell to constant T and P, will yield better signal-to-noise than an analyzer which relies on fast measurements of T and P for a real-time mole fraction calculation. Where possible, drying the air to a low, constant humidity should also be preferable to a computed water correction, so long as frequency attenuation effects of the drier are not severe. WPL corrections were applied to the DYNAMO LI7500 flux measurements, and the mean magnitude of the correction was 35 %. For the mast-mounted LI7200 we rely on the real-time computation of mole fraction from measured T and P, so WPL corrections are unnecessary.

6.2. Water Vapor Cross-Sensitivity

In addition to density effects, water vapor presents a direct interference to the CO_2 measurement in IRGA and cavity-enhanced instruments. The effect is illustrated by lab test results shown in Figure 9. The LI7200 and Picarro CRDS analyzers drew air from a common gas sample manifold. Dry air from a compressed gas cylinder had a CO_2 concentration of 423 ppm and negligible water vapor. Upon humidification to a specific humidity of $\sim$11 g kg^{-1}, the observed CRDS CO_2 concentration drops by more than 10 ppm as a result of line-broadening and dilution effects. The LI7200 mixing ratio (band broadening corrected in the analyzer, but not dilution corrected) dropped by 6.5 ppm. Application of the manufacturer's water vapor correction to the observed CRDS signal [*Rella*, 2010] yields a corrected mixing ratio very close to the original dry-air value, with a slight overcorrection bias of 0.1 ppm to 0.2 ppm. The LI7200 "dry" output (dashed green trace) yields an overcorrection bias of 1.1 ppm (0.24 %) which could arise from errors in the

LI-COR band-broadening correction and/or error in the LI7200 H_2O calibration. Humidity was independently verified with a Vaisala HMP-35 T/RH sensor, so error in the band-broadening/cross sensitivity correction may explain most of the LI7200 bias.

The true CO_2 mixing ratio may be represented as the measured value minus a factor proportional to the specific humidity, q, where μ is the proportionality or cross-correlation coefficient at zero frequency.

$$c = c_m - \mu q \tag{10}$$

Assuming the 1.1 ppm overcorrection for the in Figure 9 represents the water vapor crosstalk component in the CO_2 measurement, the LI7200 cross-correlation coefficient at constant c and q is $\mu_0 = 1.1/11 = 0.10\,\mathrm{ppm\ kg\ g^{-1}}$. Toward the end of DYNAMO Leg 3 the Nafion dryer was removed from the lab LI7200 for a direct comparison with the mast sensors (highlighted by the circled segment in Figure 2). Minus the dryer, LI7200 "dry" CO_2 mole fraction increases by $\sim$1.7 ppm. The change in q upon removing the dryer is about $17\,\mathrm{g\,kg^{-1}}$, yielding a second estimate for $\mu_0 = 0.10$, which is identical to the value observed in lab tests.

Equation (10) may be recast in flux terms [*Edson et al.*, 2011, equation A1].

$$\overline{w'c'} = \overline{w'c'_m} - \mu\,\overline{w'q'} \tag{11}$$

From 11 we therefore expect an error the in observed CO_2 flux equal to 10 % of $\overline{w'q'}$ if $\mu_0 = \mu$. Mean DYNAMO latent heat flux of $100\,\mathrm{W\,m^{-2}\,s}$ at 29 °C and 1015 mb equates to $\overline{w'q'} \approx 0.0343\,\mathrm{g\,kg^{-1}\,m\,s^{-1}}$ and an expected CO_2 flux error of $\sim 3.43 \times 10^{-3}$ ppm m/s, or about 7.3 times the median dry-air LI7200 flux of 4.7×10^{-4} ppm m/s (Table 2). Water vapor cross talk bias illustrated in Figure 9 therefore represents about half of observed error in LI7200 CO_2 flux measurements in moist air, which are biased by a factor of 14.

Figure 10 is an expanded view of CO_2 measurements for the period when the dryer was removed from the lab-mounted LI7200. In moist air, the "dry" mole fraction output of the lab LI7200 closely tracks the same output from the mast LI7200. In the published algorithm, LI-COR employs a function

$$\psi(m_w) = 1 + (a_w - 1)m_w \tag{12}$$

to obtain the corrected equivalent pressure of CO_2, where m_w is the mole fraction of water vapor and a_w is a constant specified as 1.15 for the LI7200 (see LI-COR LI-7200 Manual, equation 3-16, Publication No. 984-10564 and LI-COR Application Note 116). Recomputing the concentration from raw absorbances, using published equations and an adjustment of a_w =1.7, largely removes the offset observed in moist air (Figure 10, black trace). Similar results were obtained by doubling the LI7200 cross sensitivity factor, X_i, in equation 3-17 of the LI7200 manual. Bias in the computed dry mole fraction and excessive signal variance in moist air appears consistent across all three IRGA analyzers, but these tests are insufficient to identify the specific source of the error in the LI-COR algorithm.

The correlation (or anti-correlation) between CO_2 and H_2O flux for the mast-mounted IRGA sensors in Figure 3 indicates considerable residual water vapor crosstalk in the "corrected" LI-COR CO_2 measurements. There may be a frequency dependency to the cross-correlation coefficient, μ, if, for example, the cross sensitivity term in the LI-COR algorithm has a frequency dependence or if hygroscopic behavior of optical surface contaminants is involved. Thus, μ_0 obtained from lab tests at constant humidity will not represent the true flux error. In this case, the error cross-correlation coefficient may be

defined as

$$\mu = \frac{\int \mu(\omega) C_{wq}(\omega)}{\int C_{wq}(\omega)} \tag{13}$$

where $C_{wq}(\omega)$ is the $w'q'$ cospectrum and $\mu(\omega)$ is given by *Edson et al.* [2011, equation 22] as

$$\mu(\omega) = \left(1 - \frac{C_{qc}(\omega)}{C_{qc_m}(\omega)}\right) \frac{C_{qc_m}(\omega)}{S_{qq}(\omega)} \approx \Gamma \frac{C_{qc_m}(\omega)}{S_{qq}(\omega)} \tag{14}$$

and Γ is a frequency-independent estimate for the term in parenthesis; the difference from unity is a measure of the true atmospheric $q'c'$ cross-correlation and $\Gamma > 1$ indicates anti-correlation.

Related approaches have been published to correct water vapor crosstalk and both are applied to the LI7200 and LI7500 mast-measured fluxes in this study. The PKT method [*Prytherch et al.*, 2010b] is an iterative correction applied to the raw time series to reduce the observed dependence of CO_2 on relative humidity. The cross-correlation method [*Edson et al.*, 2011] is a spectral approach which seeks to preserve cospectral shape in the corrected result though a determination of $\mu(\omega)$ in (14). Application of the cross-correlation approach is complicated by the need to account for the real atmospheric component of $q'c'$ correlation. For SO-GasEx flux measurements, *Edson et al.* [2011] achieve best agreement with the PKT approach with $\Gamma = 0.88$. An analysis of water vapor correlation with a third, independent scalar measurement is one approach to obtain Γ, and *Edson et al.* [2011, Appendix A] illustrate the use of temperature and humidity fluctuations for this purpose. This approach was unsuccessful for DYNAMO, however, due to low sensible heat fluxes. In fact, temperature is not the best scalar for this purpose because $\overline{w'T'}$ approaches zero under near-neutral stability conditions prevalent at sea. An alternate scalar, such as dimethylsulfide, might prove more useful but was not available during

DYNAMO. Lacking an independent estimate for the true atmospheric cross-correlation, mast-measured fluxes were scaled to the dry-air LI7200 flux. Best agreement between the mast-measured and dry-air CO_2 flux is obtained with $\Gamma_{7200} = 0.93$ and $\Gamma_{7500} = 1.1$ (project average values), indicating a mean atmospheric $q'c'$ cross-correlation which is 7 % and 11 % of the observed $q'c'$ cross-correlation for these IRGA analyzers.

Cross-correlation corrected fluxes are plotted on the lower panel of Figure 3. Summary results for the PKT and cross-correlation approaches (median flux $\pm 1\sigma$) are provided in Table 2. We find the PKT method yields some improvement in flux bias but leads to significantly increased variance in the final result. It is not possible to judge the accuracy of the cross-correlation correction since agreement with mean dry-air flux is the condition used to derive Γ, but the result is indicative of the improvement in both mean flux and variance that could result where an accurate and independent determination of Γ is available. Figure 11 shows project mean cospectra for the IRGA analyzers and spectral effects of the cross-correlation correction. The water vapor crosstalk effect is observed at all frequencies across the flux measurement bandpass. Some spectral distortion is apparent in the corrected cospectra but fluxes are very small.

The source of IRGA water vapor crosstalk is often ascribed to hygroscopic contamination of optical surfaces. An analysis of the observed cross-correlation coefficient, $\mu_{obs} = \overline{q'c'_m}/\sigma_q^2$ (the first term in eq. A2, *Edson et al.* [2011]) provides a test of this hypothesis. If optical contamination is a major factor inducing cross-sensitivity, the magnitude of μ_{obs} should decrease significantly following a wash cycle on the LI7500 analyzer. In fact, we find no significant shift in μ_{obs} when lenses are cleaned with distilled water; either optical

552 contamination is not a source of $q'c'$ cross-correlation or the relevant contaminants are
553 resistant to removal by rinsing.

554 Figure 12 illustrates CRDS response to water vapor with the Nafion air dryer installed
555 in the sample air stream. As expected, the uncorrected mole fraction remains constant
556 following a large increase in water vapor. Sample dew point is held to $<-10\,°C$ under
557 all conditions, and at that level water vapor effects are negligible. A small drift in mean
558 concentration was caused by incomplete temperature and pressure equilibration of the
559 CRDS cavity at the time of the test. Lacking a water measurement, we could not test the
560 manufacturer's computed CRDS water vapor correction in the field.

6.3. Motion Related Effects for CO_2 Analyzers

561 Motion interference is an issue unique to ship and aircraft flux measurements. For
562 IRGA analyzers, this effect was noted in the earliest field studies but the exact cause
563 remains uncertain. It may be due to modulation of the chopper wheel rotation [*McGillis*
564 *et al.*, 2001a] or flexing of the source filament [*Miller et al.*, 2010]. "Zero calibrations"
565 with closed-path analyzers [*McGillis et al.*, 2001a, b] and shrouded "null" open-path
566 sensors [*Lauvset et al.*, 2011; *Edson et al.*, 2011] have both been used as experimental
567 approaches to quantify the ship-motion component of the measured flux, but computed
568 corrections in data processing algorithms are more generally useful. *Miller et al.* [2010]
569 employ a linear regression between observed CO_2 and the platform angular rates and
570 linear accelerations to remove the motion-induced signal. *Edson et al.* [2011] describe a
571 mathematically equivalent decorrelation method. For DYNAMO, a motion decorrelation
572 was applied to raw CO_2 and H_2O data prior to subsequent water vapor corrections and

573 flux computations. Cospectra in Figure 11 do not show significant motion influence,
574 illustrating the effectiveness of the motion decorrelation approach.

575 Motion interference with the CRDS analyzer is apparent in cavity pressure spectra
576 (Figure 13) and CO_2 cospectra (Figure 14), implying motion sensitivity in the pressure
577 control system. Standard CRDS pressure control uses a single DC solenoid valve. In an
578 attempt to reduce motion sensitivity, the manufacturer subsequently modified the analyzer
579 used in this study by installing two horizontally opposed valves. In theory, motion in one
580 valve is offset by countervailing motion in the opposed valve. While the modification yields
581 some improvement, TORERO results indicate it is only partially successful. The close
582 correspondence between ship motion variance and cavity pressure variance is illustrated
583 in Figure 15. In lab experiments, we find CO_2 sensitivity to changes in cavity pressure
584 is about 0.112 ppm torr^{-1}. However, excess σ_{CO_2} due to motion (the integrated area of
585 the motion peak in the CO_2 spectrum) is about 2.5 times greater than expected given
586 the observed σ_p and pressure sensitivity, so additional factors are likely involved. As with
587 the IRGA analyzers, if motion response is roughly linear it may be possible to reduce
588 or eliminate it with a regression or decorrelation approach. We plan to include a 3-axis
589 accelerometer measurement at the location of the CRDS analyzer in future deployments
590 to test this approach.

591 For TORERO, motion interference in the CRDS CO_2 measurement was most significant
592 during the outbound transit, when wind speeds were higher and the ship was making
593 maximum headway into the wind and swell. Cospectra from the low-flux, high-motion
594 transit leg and high-flux, low-motion equatorial portion of the cruise are shown in Figure
595 14. Motion interference is evident at 0.1 Hz to 0.3 Hz in the high-motion cospectrum. Flux

is computed as the integral of the cospectrum and for flux measurements where motion interference was significant (707 of 2677 samples), a corrected flux estimate was obtained by fitting a baseline under the cospectral motion peak and eliminating it from the integral computation. The mean motion correction for these flux measurements was 28 %.

One further source of error related to ship motion should be considered. We compute flux as the covariance of vertical wind and scalar measurements, $F_c = \overline{w'c'}$. Error in the wind motion correction leads to error in w', and vertical motion of the analyzer or gas inlet through the CO_2 concentration gradient above the surface adds error to c'. If wind correction error is some fraction, f_m, of the computed motion, and motions are crudely sinusoidal, fractional error from these sources is shown to be [*Blomquist et al.*, 2010]

$$\frac{\Delta F_c}{F_c} = \frac{f_m}{\kappa u_* \overline{z}} \frac{2\sigma_{w_m}^2}{\omega} \overline{\sin(\omega t)\cos(\omega t)} \tag{15}$$

where $\sigma_{w_m}^2$ is the variance of vertical motion of the sensor, $\kappa = 0.4$ is the Von Karman constant, $\overline{z}$ is mean measurement height and $\omega = 2\pi f$ is angular velocity of the motion.

Because the average of the product of sine and cosine is zero, we conclude motion and concentration terms are in quadrature and therefore do not contribute to flux. A peak at motion frequencies is, in fact, generally present in the quadrature spectrum, supporting this conclusion. However, assumptions of simple fractional dependence and sinusoidal motion are not exactly correct. For extreme high wind and motion conditions ($f_m = 0.1$ s^{-1}, $\overline{u} = 20$ $m\,s^{-1}$, $u_* = 0.8$ $m\,s^{-1}$, $\omega = 0.6$ $rad\,s^{-1}$, $\overline{z} = 18$ m, and $\sigma_{w_m}^2 = 6$ $m^2\,s^{-2}$) the relationship reduces to the following [*Blomquist et al.*, 2010].

$$\frac{\Delta F_c}{F_c} = 0.18 \left(2\overline{\sin(\omega t)\cos(\omega t)}\right) \tag{16}$$

Thus, for the unlikely case that motion and concentration are in phase rather than in quadrature (i.e. $2\overline{\sin(\omega t)\cos(\omega t)} = 1$) and motion conditions are extreme, the worst case error is $\leq$18 %. This effect will contribute a slightly increased scatter to flux measurements in heavy seas.

6.4. Spectral Attenuation

All EC flux measurements are bandwidth limited and may therefore underestimate the true surface flux [see review by *Massman and Clement*, 2004]. Resolution of the smallest eddies, at the highest frequencies, is primarily limited by sensor separation and sampling frequency, with additional low-pass filtering effects from tubing in closed-path systems. Finite flux averaging periods and mean removal or detrending methods serve to high-pass filter the lowest frequencies. Over the ocean at moderate wind speeds, under near-stationary and sufficiently turbulent conditions, a thirty minute averaging period is usually sufficient to limit the loss of low-frequency flux signal. High frequency losses in closed-path systems are a more significant problem. Two general approaches have been used to deal with spectral attenuation corrections: transfer functions [e.g. *Moore*, 1986; *Horst*, 1997; *Massman*, 2000] and spectral similarity methods [*Hicks and McMillen*, 1988].

Flux is often computed as the integral of the observed cospectrum, which can be represented as the integral of the "true" cospectrum times a transfer function, $H(f)$ [e.g. as in *Bariteau et al.*, 2010]:.

$$F_{xm} = \int_0^{f_n} C_{wxm}(f)df = \int_0^{f_n} C_{wx}(f)\,[H(f)]^{1/2}df \tag{17}$$

where the subscript m refers to the measured quantity and f_n is the Nyquist frequency. For a closed-path CO_2 analyzer subject to tube flow spectral attenuation [*Lenschow and*

Raupach, 1991], $H(f)$ may be represented by a simple first-order low-pass filter process characterized by a time constant, τ_c:

$$H(f) = \left[1 + (2\pi f \tau_c)^2\right]^{-1} \tag{18}$$

Note that in (17), we use the square root of $H(f)$ because only the CO_2 signal is attenuated; w bandwidth is not considered a limiting factor. A model of the "true" cospectrum is required in (17). The normalized flat terrain, neutral-stability scalar cospectrum of *Kaimal et al.* [1972] is often used

$$\frac{fC_{wx}(f)}{F_x} = \frac{11n}{(1+13.3n)^{1.75}} \qquad n \leq 1.0 \tag{19a}$$

$$\frac{fC_{wx}(f)}{F_x} = \frac{4.4n}{(1+3.8n)^{2.4}} \qquad n \geq 1.0 \tag{19b}$$

where the surface normalized frequency $n = fz/\overline{u}_r$.

Given an estimate for τ_c, (18) and (19) may be used to derive an estimate of flux loss from high frequency spectral attenuation:

$$R_{attn}(z, \overline{u}_r) = \frac{\int_0^{f_n} C_{wx}(f)\,[H(f)]^{1/2} df}{\int_0^{f_n} C_{wx}(f) df} \tag{20}$$

A variety of methods can be used to obtain τ_c: 1) empirical experiments to characterize the transfer function of the inlet and analyzer system [e.g. as in *Blomquist et al.*, 2010]; 2) by invoking spectral similarity, the ratio of the attenuated cospectrum and a reference non-attenuated cospectrum (usually C_{wT}) can be used to estimate the cutoff frequency, f_c – the point where the cospectral ratio drops by $1/\sqrt{2}$ from the unattenuated value – and then $\tau_c = 1/2\pi f_c$; or 3) a step impulse in CO_2 concentration can be introduced at the sample inlet tip. The resulting analyzer response can be fit to a low-pass step response

function [as in *Peters et al.*, 2001]

$$s(t) = 1 \qquad t < t_{lag} \tag{21a}$$

$$s(t) = \pm \exp\left(\frac{t_{lag} - t}{\tau_c}\right) \qquad t \geq t_{lag} \tag{21b}$$

where t_{lag} is the flow rate-dependent time delay of the inlet and the sign determines whether the step is positive or negative.

The alternate approach to attenuation corrections via spectral similarity is useful when a simultaneous high-bandwidth scalar measurement is available for comparison. Sensible heat flux or $\overline{w'T'}$, as measured by the sonic anemometer, is often used for this purpose. Water vapor flux from an open path sensor (e.g. LI7500) is also suitable, and may be preferable when $\overline{w'T'}$ is near zero. The correction factor is computed by scaling the normalized attenuated scalar cospectrum to the normalized reference $w'T'$ cospectrum. Frequently, a subrange of unattenuated frequencies within the cospectrum is chosen as the basis for the scaling. Computation of the Ogives has also been employed as an expedient for similarity scaling in several recent reports of flux measurements with closed-path sensors [*Spirig et al.*, 2005; *Ammann et al.*, 2006; *Miller et al.*, 2010]. In addition to providing a basis for spectral attenuation corrections, the Ogive indicates if averaging time is sufficient to capture low frequency flux signal.

The Ogive is defined as the cumulative sum (integral) of the cospectrum [*Oncley*, 1989] from $f = 0$ to f_n and may be computed from a cospectrum averaged into n frequency bins on a log scale:

$$Og_{wx}(f_m) = \sum_{i=0}^{m} Co_{wx}(f_m)\Delta f_m \tag{22a}$$

$$m = 0, 1, 2, \ldots, n \tag{22b}$$

Normalized to total flux, and plotted together versus log frequency, the Ogive for the attenuated signal lies above the reference Ogive curve. The mean ratio of normalized Ogives,

$$R_{attn}(f) = \frac{Og_{wT}(f) \,/\, \overline{w'T'}}{Og_{wco_2}(f) \,/\, \overline{w'co_2'}} \tag{23}$$

over a range of frequencies where both measurements are assumed to be similar and unattenuated (typically 0.01 Hz to 0.1 Hz) is an estimate for the flux attenuation factor [see *Spirig et al.*, 2005; *Ammann et al.*, 2006].

For the LI7200 and CRDS closed-path analyzers in this study, a "puff" system was used to synchronize wind and CO_2 measurements, providing a convenient way to determine τ_c. A burst of nitrogen or compressed air from a solenoid valve, driven by a square-wave trigger with a period of 3 s to 5 s, is injected near the sample inlet tip at the beginning of each hour. The corresponding pulse in CO_2 response was matched to the recorded trigger pulse to determine inlet delay time. A low-pass response function (21) was fit to the rising (valve closure) edge of hourly pulses to determine τ_c. In this the case the second step response, when the valve closes, is judged a better representation of an ideal step impulse than the valve opening, which tends to overshoot due to the initial pressure surge. For TORERO, the mean time constant determined over 705 hours of measurements was $\tau_c = 0.126 \pm 0.008$ s ($f_c = 1.26$ Hz). Values were consistent over the entire project. Attenuation corrections computed from (20) and shown in Figure 16 represent a 5 % to 6 % correction when $\overline{u}_r = 12\,\mathrm{m\,s^{-1}}$ to $14\,\mathrm{m\,s^{-1}}$ and ∼1 % when $\overline{u}_r = 3\,\mathrm{m\,s^{-1}}$ to $5\,\mathrm{m\,s^{-1}}$. For DYNAMO, analysis of "puff" system response for the LI7200 lab analyzer yields $t_{lag} =$ 6.2±0.2 s and τ_c =0.38±0.06 s yielding a mean attenuation correction of ∼7 %.

Generally low sensible heat flux during TORERO limited the application of spectral similarity methods. As shown in Figure 4, $\overline{w'T'}$ observations were scattered about zero and generally smaller than $\pm 0.01\,^{\circ}\mathrm{C\,m\,s^{-1}}$. This is typical for the tropics, where sensible heat flux is much smaller than latent heat flux. Water vapor flux measurements were not available for TORERO. Figure 17 shows the ratio of normalized cospectra and Ogives for a period when both $\overline{w'T'}$ and $\overline{w'\mathrm{CO_2}'}$ yield reasonable cospectra. The Ogives cleanly approach the asymptote at both ends, indicating the measurement successfully captured turbulence frequencies contributing to the flux. The normalized Ogive curves are identical within the precision of the data, however, and it is difficult to determine an attenuation factor by scaling the two curves. From the cospectral ratio plot in Figure 17, it appears f_c should be near 1 Hz, but excessive noise again prevents a precise confirmation of τ_c by this method. Time constants from "puff" pulses over the same period yield an attenuation correction of $\sim$2.5 %. It is reasonable to expect some degree of spectral attenuation with the inlet tubing and dryer. For DYNAMO and TORERO, τ_c determined hourly from the step impulse response (as in Figure 16) is judged a more reliable measure of the attenuation correction.

Spectral attenuation is wind speed dependent, but even when $u > 15\,\mathrm{m\,s^{-1}}$ flux bias is less than 20 % so long as the inlet flow is fully turbulent. If the attenuation correction is precise to about the same degree, residual bias in the flux estimate will be less than 5 %. We note that gases which adsorb or condense on tubing surfaces, such as water vapor, are the exception. Frequency attenuation can be much worse and variable, especially as tubing surfaces become coated with grime and hygroscopic contaminants [see *Leuning and Judd*, 1996; *Peters et al.*, 2001], which happens rapidly at sea. For this reason, open-path

sensors are preferred for water vapor flux. EC measurements of soluble or reactive trace gases using long sample lines may also be problematic.

6.5. Wind-Motion Crosstalk

Correcting measured wind velocities for ship motion typically requires a strapped-down motion sensor at the location of the anemometer, providing angular rotation rate (or tilt angle) and acceleration on three orthogonal axes. The motion correction is computed by: 1) adjusting wind vectors and accelerations for angular tilt with respect to the gravity vector; 2) integrating acceleration on all axes to yield platform velocities in earth-referenced coordinates and then; 3) subtracting platform velocities from observed, rotated winds [*Fujitani*, 1985; *Edson et al.*, 1998; *Takahashi et al.*, 2005]. A modified correction algorithm has been developed for the situation where axes of the anemometer and motion sensors are not well aligned [*Miller et al.*, 2008]. In principle, this correction should be exact. In practice, calibration bias in the wind and motion measurements and imperfections in digital filtering and numerical integrations lead to errors in the motion-corrected winds.

A sample w spectrum from TORERO in Figure 18 illustrates the large component of motion variance in observed vertical wind speeds. In this case, application of the *Edson et al.* [1998] correction scheme removes 96 % of the motion variance peak, leaving a small residual at 0.2 Hz (Figure 18 red trace, note the logarithmic scale). Much of this residual can be removed with a decorrelation or linear regression procedure along the lines of *Edson et al.* [2011] or *Miller et al.* [2010]. It should be noted, however, that some portion of the peak in w variance at 0.1 Hz to 0.2 Hz may be due to the real effects of swell on the overlying air column. The correlation between vertical ship motion and swell is often poor, but to the extent that swell and motion correlate, the decorrelation will also remove

a portion of the real response. This bias is greatest for measurements near the surface and may be a minor concern for wind measurements at 20 m.

Adopting the decorrelation approach for this example, we assume the observed vertical wind velocity is a combination of the true velocity and motion error components which are proportional to platform acceleration and velocity on the z-axis

$$w'_{obs} = w'_{true} + \mu_{a_z} a'_z + \mu_{v_z} v'_z \tag{24}$$

where a is acceleration, v is velocity, the prime represents deviation from the mean, and μ are the proportionality coefficients quantifying each motion-crosstalk component. μ coefficients are defined as covariance of observed vertical wind and z-axis vertical motion divided by the variance in vertical motion. For example, the correlation coefficient between w and z-axis velocity is:

$$\mu_{v_z} \equiv \frac{\overline{w' v'_z}}{\sigma^2_{v_z}} \tag{25}$$

An equivalent spectral representation of (24) and (25) is given in *Edson et al.* [2011]. Decorrelation of motion-corrected $w'(t)$ with respect to $a'_z(t)$ and $v'_z(t)$ via (24) provides an improved estimate for $w'(t)$ (Figure 18, green trace), yielding a significant reduction in flux-motion crosstalk. Residual motion interference in the Figure 14 high-motion cospectrum is likely the result of a correlation between w' and motion-induced error in co_2'.

6.6. Flow Distortion

Wind speed is the most significant factor driving air-sea fluxes, therefore precise measurements of 10-meter mean wind speed are important. Unfortunately, flow distortion produces a bias in mean wind speeds observed from ships. The effects of flow distortion on wind and flux measurements for individual ships has been the focus of several stud-

ies employing experimental and computational fluid dynamics (CFD) approaches [*Brut et al.*, 2002, 2005; *Dupuis et al.*, 2003; *Moat et al.*, 2006a, b; *Pedreros et al.*, 2003; *Popinet et al.*, 2004; *Weill et al.*, 2003; *Yelland et al.*, 1998, 2002]. For example, on AGOR-23 class research vessels like the R/V Roger Revelle, wind speed bias is approximately −3% and vertical displacement is about 0.7 m at the flux sensor position on the forward jackstaff for bow-on wind [see *Yelland et al.*, 2002, results for R/V Ron Brown]. This degree of error should be considered a "best case" scenario. Flow distortion is a function of relative wind direction and generally becomes more severe for side-on flow. A correction should therefore be applied to observed mean wind speeds when CFD results are available for a particular ship.

Flow distortion is also a potential source of bias in flux measurements, and minimizing its influence requires precise orientation of the measurement coordinate system [*Finnigan*, 2004, and references therein]. For our purposes, the horizontal plane of the wind sensor coordinates should be parallel to mean streamline flow over the ocean surface. Tilt in the anemometer mount and flow distortion over nearby obstacles are common problems, and flow over obstacles produces both streamline distortion and turbulent eddies. The effects of streamline distortion extend over a greater distance than turbulent eddies generated in the wake of an obstacle. While streamline distortion is correctable, it is not possible to correct for the effects of turbulence generated by obstructions, and sensors should be located far enough from an obstacle to avoid this condition.

In general, flow distortion error is greatest for momentum flux measurements due to the dependence on horizontal wind speed [e.g. *Pedreros et al.*, 2003]; observed u_* typically shows a trend with respect to relative wind direction, indicative of this error. The effect

on scalar fluxes, while generally smaller, may still be significant. Double-rotation (DR) or planar-fit (PF) methods are routinely used to correct coordinate tilt prior to computing flux [*Wilczak et al.*, 2001; *Finnigan*, 2004]. On a ship, the motion correction process removes bias in the wind data from tilt in the anemometer mount, bringing coordinates into alignment with the gravity vector. Flow distortion over the ship superstructure remains, however. A DR tilt correction has been applied to data in this study to bring the wind measurements into the streamlines. Valid flux measurements are further limited to minimally distorted wind sectors, usually $\pm$ 60° to 90° from the bow.

There are, however, potential problems applying DR tilt corrections in circumstances of substantial obstacle-induced flow distortion, where tilt angle displays a strong dependence on wind direction; it may not be appropriate to force $\overline{w} = 0$ over the entire flux measurement interval, and procedures to circumvent this limitation have been investigated [e.g. *Klipp*, 2004]. *Griessbaum and Schmidt* [2009] recently examined the effects of severe flow distortion on momentum, buoyancy and scalar fluxes, proposing an improved flow distortion correction based on detailed large-eddy simulaton (LES) modeling. In their approach, LES modeling of the measurement site, including all significant local obstructions, is used to derive a set of correction factors, $(f_u, f_v, f_w)_j$, computed over a range of j relative wind directions in 5° increments. These correction factors are applied in a time-dependent manner to the raw 10 Hz wind data. This method allows "an estimate of the undisturbed mean geometry of the mean wind field as it was before approaching any nearby obstructions", and they demonstrate a 5 % to 15 % difference in CO_2 flux between standard tilt corrections and their time-dependent distortion correction scheme. They employ a DR or PF tilt correction as a second step, removing bias related to tilt

817 in the anemometer mount, but this may not be necessary for ship measurements with
818 motion-corrected raw winds.

819 The *Griessbaum and Schmidt* [2009] approach has not yet been applied to ship measure-
820 ments. Significant effort will need to be invested in CAD modeling and LES simulations.
821 While computationally intensive, LES-derived wind direction dependent correction fac-
822 tors may be advantageous in situations of moderate-to-severe distortion – on icebreakers,
823 for example, or where the measurement location is otherwise disturbed by unavoidable
824 nearby obstacles. Once computed, LES correction factors may be applied to reprocess
825 existing datasets.

6.7. Stationarity, Homogeneity and Entrainment

826 While not an instrumental issue, evaluation of meteorological stationarity is an essential
827 aspect of flux measurements. The use of theoretical cospectral models, such as *Kaimal*
828 *et al.* [1972], and invocations of spectral similarity are only valid for steady-state con-
829 ditions. In general, covariance flux at height z is only equated to the true surface flux
830 under stationary, homogeneous conditions when there is no significant difference between
831 entrainment flux at the marine boundary layer inversion and surface flux [*Businger*, 1986].
832 This is especially important in circumstances where fluxes are small and the magnitude of
833 surface flux derived scalar variance is a minute fraction of the mean background concen-
834 tration. *Miller et al.* [2010] report a large fraction of air-sea CO_2 flux measurements were
835 discarded on the basis of stationarity criteria and *Blomquist et al.* [2012] show a similar
836 sensitivity to stationarity issues in the measurement of air-sea carbon monoxide flux.

837 The evaluation of steady-state conditions tends to rely on somewhat subjective criteria.
838 One widely used test for stationarity over the averaging interval is based on the fractional

difference in covariance flux over 5- and 30-minute timescales [*Gurjanov et al.*, 1986; *Foken and Wichura*, 1996; *Lee et al.*, 2004]. It is suggested that conditions are stationary when the following ratio is less than 0.3

$$RN_{cov} = \left| \frac{\overline{(\overline{w'x'})_5} - (\overline{w'x'})_{30}}{(\overline{w'x'})_{30}} \right| \leq 0.3 \tag{26}$$

where the numerator in (26) is the difference between the 30-minute covariance and the mean covariance from 5-minute sub-intervals of the same 30-minute data segment. In essence, this test specifies the flux fraction contributed by frequencies from ∼0.001 Hz to 0.007 Hz should be less than 30 % of the 30-minute covariance flux value. The actual proportion of the flux signal expected at these frequencies is of course dependent on conditions. To be consistent, wind speed, measurement height and stability could be considered when specifying the length of the sub-interval. In practice, the test in the form given above is routinely used as a rough filter for non-steady-state conditions.

Among TORERO 30-minute flux results passing relative wind and heading criteria ($N = 2352$) we find 165 observations exceed the 30 % limit in (26). However, a few obvious outliers manage to pass the test – measurements where a single 30-minute value exceeds adjacent values by more than a factor of four – and many values near the flux detection limit are discarded which are not otherwise obviously bad. Figure 19 shows the time series of measurements over a 3-day period when CO_2 flux was essentially zero. Points in red fail the equation (26) test, presumably due to random low-frequency noise in measurements at or below the detection limit. Normally, it is desirable to retain these measurements.

Limiting the time-rate-of-change in the scalar variable ($\partial CO_2/\partial t$) is another test often used to screen for non-steady-state conditions. For DYNAMO and TORERO, the lin-

ear trend is removed from each flux data segment and the slope retained as a measure of $\partial CO_2/\partial t$. We have extended this test by including consideration of horizontal flux components, $\overline{u'co_2'}$ and $\overline{v'co_2'}$. Figure 20 shows the distribution of horizontal flux with respect to $\partial CO_2/\partial t$ on TORERO for 2352 30-minute measurements passing relative wind direction criteria. Limits on $\overline{u'co_2'}$ and $\overline{v'co_2'}$ of ± 0.025 ppm m s^{-1} and on $\partial CO_2/\partial t$ of ± 0.5 ppm hr^{-1} were chosen to exclude measurements with a significant departure from the mean (shown as a bounding box in Figure 20) . Admittedly, these limits are also subjective. Applying this test, 72 of 2352 measurements are rejected, including almost all obvious outliers. Most results near the detection limit are retained. Flux measurements discarded by these criteria are illustrated in Figure 21 for a period of significant flux variability near the end of the TORERO cruise. For DYNAMO, similar limits were applied, removing 5 % of 10-minute dry-air flux measurements from the lab LI7200 which pass other basic criteria.

It should be noted subjective limits on the magnitude of horizontal flux in this report are about ten times greater than the range in vertical flux values from Figure 4, and the limit of $\partial CO_2/\partial t < 0.5$ ppm hr^{-1} is a very small gradient; at $\overline{u}$ =8 m s^{-1} it represents an along-wind spatial gradient of about 1 ppm or 0.25 % of the mean background CO_2 concentration per 60 km. This implies weak spatial gradients in CO_2 can drive a signal variance from horizontal turbulent flux many times larger than the CO_2 variance from surface flux. A similar situation has been reported for CO flux measurements at sea [*Blomquist et al.*, 2012]. Therefore, care should be exercised in choosing the location for field studies; areas affected by even moderate to low levels of continental pollution,

for example, will provide fewer instances of suitable steady-state conditions, and a large fraction of measurements will be discarded.

Entrainment is an additional source of bias if a significant flux gradient develops between the ocean surface and marine boundary layer inversion. For CO_2, this may become a problem when pollution above the boundary layer subsides and is entrained. The situation is difficult to assess from surface measurements alone. Presumably, pollution entrainment leads to increased CO_2 variability, and appropriate stationarity criteria, as discussed above, also serve to limit flux bias from entrainment.

7. Discussion and Recommendations

7.1. Measurement System

[PROVISIONAL RECOMMENDATIONS PENDING FURTHER DISCUSSION]

This study provides further confirmation that water vapor interference is the most significant factor limiting precision and accuracy for ship-based CO_2 flux studies. These results are not definitive with respect to the cause of excessive water vapor crosstalk in the IRGA analyzers, but the interference is apparent in both LI7500 and LI7200 models. Computed CO_2 band broadening and dilution corrections in the LI-COR algorithm appear to be insufficiently precise for measurements of air-sea gas transfer and we cannot recommend CO_2 flux measurements in moist air with the IRGA instruments. We were not able to test real-time water vapor corrections for the CRDS analyzer due to the lack of a H_2O channel in our instrument. However, it is clear the dryer does not significantly compromise frequency response and there is much to be gained from removing the water vapor crosstalk and WPL correction issues altogether, whichever analyzer is used.

There may be conditions where space and power requirements of a closed-path analyzer, sample pump and dryer will present difficulties – on buoys, near-shore towers or for long-term unattended operation, for example. In this case there appears to be little recourse to the open-path analyzer, or if power is sufficient, the LI7200, but complex corrections will be required [e.g. *Prytherch et al.*, 2010b], measurement precision will be poor and a significant fraction of the observations may be discarded.

At high flow rates, long sample lines do not significantly degrade flux measurements with closed-path analyzers. If pressure drop at the analyzer is a concern, empirical tests can determine the optimal trade-off between frequency attenuation and analyzer performance. Cavity-enhanced analyzers normally operate at low pressure and seem to tolerate considerable pressure drop in the sample line. There are a variety of approaches to determine frequency attenuation and lag time; hourly gas pulses at the sample inlet have proven most useful in our work, albeit at the expense of greater measurement system complexity. However, it seems worthwhile to verify attenuation corrections with spectral similarity methods when possible. In this respect, it is an advantage to deploy the OP-IRGA for latent heat flux measurements because sensible heat flux is often quite small.

[OTHER MEASUREMENT SYSTEM RECOMMENDATIONS...]

7.2. Data Processing

Dry-air measurement with a closed-path analyzer obviates WPL, dilution and water vapor cross-talk corrections, which are the most significant source of poor flux precision and bias. The use of a dryer, therefore, greatly simplifies data processing. [FOR CASES WHERE H2O CROSSTALK CORRECTIONS ARE REQUIRED, WHAT SHALL WE RECOMMEND?]

The issue of motion interference remains a concern for all analyzers studied to-date. While adjustments to cospectral shape can be used to correct motion artifacts, application of motion decorrelation or regression methods to the raw CO_2 time series is a fundamentally superior approach. These corrections have been demonstrated for IRGA analyzers [*Miller et al.*, 2010; *Edson et al.*, 2011] and may also be applicable to the CRDS. In the future, analyzer design modifications may reduce or eliminate this problem. We did not test an OA-ICOS cavity-enhanced analyzer for this work. However, CO flux measurements at sea have been reported for this instrument, without significant motion sensitivity issues [*Blomquist et al.*, 2012].

In most cases, the issue of flow distortion is a minor factor in flux error but may become more important on larger ships or more restrictive installation environments. The inclusion of flux measurements on icebreakers for polar gas exchange studies is an obvious example. The application of CFD and LES modeling to flow distortion corrections should be considered for these cases.

[WHAT SHALL WE CONCLUDE REGARDING STEADY-STATE CRITERIA? IS THERE A THEORETICALLY SOUND, OBJECTIVE, QUANTITATIVE APPROACH TO RECOMMEND OR IS IT SUFFICIENT TO EMPLOY SOMEWHAT SUBJECTIVE CRITERIA SO LONG AS THE REASONING IS CLEARLY PRESENTED?]

8. Summary Conclusions

[SUMMARY PARAGRAPHS: ISSUES, RESULTS, RECOMMENDATIONS, PENDING COAUTHOR COMMENTS.]

Acknowledgments. (Text here)

References

947 Ammann, C., A. Brunner, C. Spirig, and A. Neftel (2006), Technical note: Water vapor
948 concentration and flux measurements with ptr-ms, *Atmos. Chem. Phys.*, *6*, 4643–4651,
949 doi:www.atmos-chem-phys.net/6/4643/2006/.

950 Auble, D. L., and T. P. Meyers (1992), An open path, fast response infrared absorption
951 gas analyzer for h2o and co2, *Bound.-Layer Meteor.*, *59*, 243–256.

952 Baer, D. S., J. B. Paul, M. Gupta, and A. O'Keefe (2002), Sensitive absorption measure-
953 ments in the near-infrared region using off-axis integrated-cavity-output spectroscopy,
954 *Appl. Phys. B*, doi:10.1007/s00340-002-0971-z.

955 Baldocchi, D., et al. (2001), Fluxnet: A new tool to study the temporal and spatial
956 variability of ecosystem-scale carbon dioxide, water vapor, and energy flux densities,
957 *Bull. Am. Met. Soc.*, *82*(11), 2415–2434.

958 Bariteau, L., D. Helmig, C. W. Fairall, J. E. Hare, J. Hueber, and E. K. Lang (2010), De-
959 termination of oceanic ozone deposition by ship-borne eddy covariance measurements,
960 *Atmos. Meas. Tech.*, *3*, 441–455, doi:www.atmos-meas-tech.net/3/441/2010/.

961 Blomquist, B. W., B. J. Huebert, C. W. Fairall, and I. C. Faloona (2010), Determining
962 the air-sea flux of dimethylsulfide by eddy correlation using mass spectroscopy, *Atmos.*
963 *Meas. Tech.*, *3*, 1–20, doi:www.atmos-meas-tech.net/3/1/2010/.

964 Blomquist, B. W., C. W. Fairall, B. J. Huebert, and S. T. Wilson (2012), Direct measure-
965 ment of the oceanic carbon monoxide flux by eddy correlation, *Atmos. Meas. Tech.*, *5*,
966 3069–3075, doi:10.5194/amt-5-3069-2012.

967 Brut, A., A. Butet, S. Planton, P. Durand, and G. Caniaux (2002), Influence of the airflow
968 distortion on air–sea flux measurements aboard research vessel: Results of physical

969 simulations applied to the equalant99 experiment, in *Preprints, 15th Symposium on*
970 *boundary laters and turbulence*, pp. 147–150, Wageningen, The Netherlands.

971 Brut, A., A. Butet, P. Durand, G. Caniaux, and S. Planton (2005), Air–sea exchanges
972 in the equatorial area from the equalant99 dataset: Bulk parametrizations of turbulent
973 fluxes corrected for airflow distortion, *Q. J. Royal Met. Soc.*, *131*, 2497–2538, doi:
974 10.1256/qj.03.185.

975 Businger, J. A. (1986), Evaluation of the accuracy with which dry deposition can be
976 measured with current micrometeorological techniques, *J. Climate Appl. Meteorol.*, *25*,
977 1100–1124.

978 Dupuis, H., C. Guerin, D. Hauser, A. Weill, P. Nacass, W. M. Drennan, S.Cloche, and
979 H. C. Graber (2003), Impact of flow distortion corrections on turbulent fluxes estimated
980 by the inertial dissipation method during the fetch experiment on the r/v l'atalante, *J.*
981 *Geophys. Res.*, *108*(C3), 8064, doi:10.1029/2001JC001075.

982 Edson, J. B., A. A. Hinton, K. E. Prada, J. E. Hare, and C. W. Fairall (1998), Direct
983 covariance flux estimates from mobile platforms at sea, *J. Atmos. Oceanic Technol.*, *15*,
984 547–562.

985 Edson, J. B., C. W. Fairall, L. Bariteau, C. J. Zappa, A. Cifuentes-Lorenzen, W. R.
986 McGillis, S. Pezoa, J. E. Hare, and D. Helmig (2011), Direct covariance measurement
987 of co2 gas transfer velocity during the 2008 southern ocean gas exchange experiment:
988 Wind speed dependency, *J. Geophys. Res.*, *116*(C00F10), doi:10.1029/2011JC007022.

989 Fairall, C. W., A. B. White, J. B. Edson, and J. E. Hare (1997), Integrated shipboard
990 measurements of the marine boundary layer, *J. Atmos. Oceanic Technol.*, *14*, 338–359.

991 Fairall, C. W., J. E. Hare, J. E. Edson, and W. McGillis (2000), Parameterization and
992 micrometeorological measurement of air-sea gas transfer, *Bound.-Layer Meteor.*, *96*,
993 63–105.

994 Fairall, C. W., E. F. Bradley, J. E. Hare, A. A. Grachev, and J. B. Edson (2003), Bulk
995 parameterization of air-sea fluxes: Updates and verification for the COARE algorithm,
996 *J. Climate*, *16*, 571–591.

997 Fairall, C. W., et al. (2011), Implementation of the coupled-ocean-atmosphere respones
998 experiment algorithm with co_2, dimethyl sulfide, and o_3, *J. Geophys. Res.*, *116*(C00F09),
999 doi:10.1029/2010JC006884.

1000 Finnigan, J. J. (2004), A re-evaluation of long-term flux measurement techniques part ii:
1001 Coordinate systems, *Bound.-Layer Meteor.*, *113*, 1–41.

1002 Foken, T., and B. Wichura (1996), Tools for quality assessment of surface-based flux
1003 measurements, *Ag. For. Met.*, *78*, 83–105.

1004 Fujitani, T. (1985), Method of turbulent flux measurement on a ship using a stable plat-
1005 form system, *Pap. Meteorol. Geophys.*, *36*, 157–170.

1006 Griessbaum, F., and A. Schmidt (2009), Advanced tilt correction from flow distortion
1007 effects on turbulent co2 fluxes in complex environments using large eddy simulation, *Q.*
1008 *J. Royal Met. Soc.*, *135*, 1603–1613, doi:10.1002/qj.472.

1009 Griffis, T. J., S. D. Sargent, J. M. Baker, X. Lee, B. D. Tanner, J. Greene, E. Swiatek,
1010 and K. Billmark (2008), Direct measurement of biosphere-atmosphere isotopic co2
1011 exchange using eddy covariance technique, *J. Geophys. Res.*, *113*, D08,304, doi:
1012 10.1029/2007JD009297.

1013 Gurjanov, A. E., S. L. Zubkovskij, and M. M. Federov (1986), 'mnogokanalnaja avtoma-
1014 tizirovannaja sistema obrabotki signalov na baze', *EVM. Geod. Geophys. Veroff.*, *R. II*
1015 *26*, 17–20.

1016 Hicks, B. B., and R. T. McMillen (1988), On measurement of dry deposition using im-
1017 perfect sensors and in non-ideal terrain, *Bound.-Layer Meteor.*, *42*, 79–84.

1018 Ho, D. T., C. S. Law, M. J. Simth, P. Schlosser, M. Harvey, and P. Hill (2006), Measure-
1019 ments of air-sea gas exchange at high wind speeds in the southern ocean: Implications
1020 for global parameterizations, *Geophys. Res. Lett.*, *33*, L16,611.

1021 Ho, D. T., R. Wanninkhof, P. Schlosser, D. S. Ullman, D. Hebert, and K. F. Sullivan
1022 (2011), Toward a universal relationship between wind speed and gas exchange: Gas
1023 transfer velocities measured with 3he/sf6 during the southern ocean gas exchange ex-
1024 periment, *J. Geophys. Res.*, *116*, C00F04.

1025 Horst, T. W. (1997), A simple formula for attenuation of eddy fluxes measured with
1026 first-order-response scalar sensors, *Bound.-Layer Meteor.*, *82*, 219–233.

1027 Jacobson, A. R., S. E. M. Fletcher, N. Gruber, J. L. Sarmiento, and M. Gloor (2007), A
1028 joint atmosphere-ocean inversion for surface fluxes of carbon dioxide: 1. methods and
1029 global-scale fluxes, *Global Biogeochem. Cycles*, *21*, GB1019, doi:10.1029/2005GB002556.

1030 Jones, E. P., T. V. Ward, and H. H. Zwick (1978), A fast response atmospheric co2 sensor
1031 for eddy correlation measurements, *Atmos. Environ.*, *12*, 845–851.

1032 Kaimal, J. C., J. C. Wyngaard, Y. Izumi, and O. R. Cote (1972), Spectral characteristics
1033 of surface-layer turbulence, *Q. J. Royal Met. Soc.*, *98*, 563–589.

1034 Klipp, C. (2004), A generalized planar fit method for sonic anemometer tilt correction, in
1035 *Preprints, 16th Symposium on boundary layers and turbulence*, Portland, Maine.

1036 Kohsiek, W. (1991), Infrared h2o/co2 sensor with fiber optics, in *Proceedings of the Sev-*
1037 *enth Symposium on Meteorological Observations and Instrumentation*, 14-18 January,
1038 New Orleans, LA, pp. 352–355, Amer. Meteorol. Soc.

1039 Kohsiek, W. (2000), Water vapor cross-sensitivity of open path h2o/co2 sensors, *J. Atmos.*
1040 *Oceanic Technol.*, *17*, 299–311.

1041 Kondo, F., and O. Tsukamoto (2007), Air-sea flux by eddy covariance technique in the
1042 equatorial indian ocean, *J. Oceanography*, *63*, 449–456.

1043 Kowalski, A. S., and D. Argueso (2011), Scalar arguments of the mathematical functions
1044 defining molecular and turbulent transport of heat and mass in compressible fluids,
1045 *Tellus*, *63B*, 1059–1066, doi:10.1111/j.1600-0889.2011.00579.x.

1046 Lauvset, S. K., W. R. McGillis, L. Bariteau, C. W. Fairall, T. Johannessen, A. Olsen,
1047 and C. J. Zappa (2011), Direct measurements of co2 flux in the greenland sea, *Geophys.*
1048 *Res. Lett.*, *38*(L12603), doi:10.1029/2011GL047722.

1049 Lee, X., and W. J. Massman (2011), A perspective on thrity years of the webb, pearman,
1050 and leuning density corrections, *Bound.-Layer Meteor.*, *139*, 37–59, doi:10.1007/s10546-
1051 010-9575-z.

1052 Lee, X., W. Massman, and B. Law (Eds.) (2004), *Handbook of micrometeorology: a guide*
1053 *for surface flux measurement and analysis*, Kluwer Academic Publishers.

1054 Lenschow, D. H., and M. R. Raupach (1991), The attenuation of fluctuations in scalar
1055 concentrations through sampling tubes, *J. Geophys. Res.*, *96*(D8), 15,259–15,268.

1056 Leuning, R., and M. J. Judd (1996), The relative merits of open- and closed-path analysers
1057 for measurement of eddy fluxes, *Global Change Biology*, *2*, 241–253.

1058 Massman, W. J. (2000), A simple method for estimating frequency response corrections
1059 for eddy covariance systems, *Ag. For. Met.*, *104*, 185–198.

1060 Massman, W. J., and R. Clement (2004), Uncertainty in eddy covariance flux estimates
1061 resulting from spectral attenuation, in *Handbook of micrometeorology: a guide for sur-*
1062 *face flux measurement and analysis*, edited by X. Lee, W. J. Massman, and B. Law, pp.
1063 67–99, Kluwer Academic Publishers.

1064 Massman, W. J., and X. Lee (2002), Eddy covariance flux corrections and uncertainties
1065 in long-term studies of carbon and energy exchanges, *Ag. For. Met.*, *113*, 121–144.

1066 McGillis, W. R., J. B. Edson, J. E. Hare, and C. W. Fairall (2001a), Direct covariance
1067 air-sea co2 fluxes, *J. Geophys. Res.*, *106*, 16,729–16,745.

1068 McGillis, W. R., J. B. Edson, J. D. Ware, J. W. H. Dacey, J. E. Hare, C. W. Fairall, and
1069 R. Wanninkhof (2001b), Carbon dioxide flux techniques performed during GasEx-98,
1070 *Mar. Chem.*, *75*, 267–280.

1071 McGillis, W. R., et al. (2004), Air-sea co2 exchange in the equatorial pacific, *J. Geophys.*
1072 *Res.*, *109*, C08S02, doi:10.1029/2003JC002256.

1073 Miller, S., C. Marandino, W. de Bruyn, and E. S. Saltzman (2009), Air-sea exchange of
1074 co2 and dms in the north atlantic by eddy covariance, *Geophys. Res. Lett.*, *36*, L15,816,
1075 doi:10.1029/2009GL038907.

1076 Miller, S. D., T. S. Hristov, J. B. Edson, and C. A. Friehe (2008), Platform motion effects
1077 on measurements of turbulence and air-sea exchange over the open ocean, *J. Atmos.*
1078 *Oceanic Technol.*, *25*, 1683–1694, doi:10.1175/2008JTECHO547.1.

1079 Miller, S. D., C. Marandino, and E. S. Saltzman (2010), Ship-based measurement
1080 of air-sea co2 exchange by eddy covariance, *J. Geophys. Res.*, *115*, D02,304, doi:

10.1029/2009JD012193.

Moat, B. I., M. J. Yelland, R. W. Pascal, and A. F. Molland (2006a), Quantifying the airflow distortion over merchant ships. part i: Validation of a cfd model., *J. Atmos. Oceanic Technol.*, *23*, 341–350.

Moat, B. I., M. J. Yelland, and A. F. Molland (2006b), Quantifying the airflow distortion over merchant ships. part ii: Application of the model results, *J. Atmos. Oceanic Technol.*, *23*, 351–360.

Moore, C. J. (1986), Frequency response corrections for eddy correlation systems, *Bound.-Layer Meteor.*, *37*(1-2), 17–35, doi:10.1007/BF00122754.

Nakai, T., H. Iwata, and Y. Harazono (2011), Importance of mixing ratio for a long-term co2 flux measurement with a closed-path system, *Telluis*, *63B*, 302–308, doi: 10.1111/j.1600-0889.2011.00538.x.

Nightingale, P. D., G. Malin, C. S. Law, A. J. Watson, P. S. Liss, M. I. Liddicoat, J. Boutin, and R. C. Upstill-Goddard (2000), In situ evaluation of air-sea gas exchange parameterizations using novel conservative and volatile tracers, *Global Biogeochem. Cycles*, *14*, 373–387.

Ohtaki, E., and T. Matsui (1982), Infrared device for simultaneous measurement of fluctuations of atmospheric carbon dioxide and water vapor, *Bound.-Layer Meteor.*, *24*, 109–119.

O'Keefe, A., and D. A. G. Deacon (1988), Cavity ring-down optical spectrometer for absorption measurements using pulsed laser sources, *Rev. Sci. Inst.*, *59*(12), 2544–2551.

O'Keefe, A., J. J. Scherer, and J. B. Paul (1999), Cw integrated cavity output spectroscopy, *Chem. Phys. Lett.*, *307*, 343–349.

1104 Oncley, S. P. (1989), Parameterization techniques in the atmospheric surface layer, Ph.D.
1105 thesis, University of California, Irvine.

1106 Pedreros, R., G. Dardier, H. Dupuis, H. C. Graber, W. M. Drennan, A. Weill, C. Guerin,
1107 and P. Nacass (2003), Momentum and heat fluxes via the eddy correlatin method
1108 on the r/v l'atalante and an asis buoy, *J. Geophys. Res.*, *108*(C11), 3339, doi:
1109 10.1029/2002JC001449.

1110 Peters, G., B. Fischer, and H. Munster (2001), Eddy covariance measurements with closed-
1111 path optical humidity sensors: A feasible concept?, *J. Atmos. Oceanic Technol.*, *18*,
1112 503–514.

1113 Popinet, S., M. Smith, and C. Stevens (2004), Experimental and numerical study of
1114 the turbulence characteristics of airflow around a research vessel, *J. Atmos. Oceanic*
1115 *Technol.*, *21*, 1575–1589.

1116 Prytherch, J., M. J. Yelland, R. W. Pascal, B. I. Moat, I. Skjelvan, and V. A. Srokosz
1117 (2010a), Open ocean gas transfer velocity derived from long-term direct measurements
1118 of the co2 flux, *Geophys. Res. Lett.*, *37*, L23,607, doi:10.1029/2010GL045597.

1119 Prytherch, J., M. J. Yelland, R. W. Pascal, B. I. Moat, I. Skjelvan, and C. C. Neill (2010b),
1120 Direct measurements of the co2 flux over the ocean: Development of a novel method,
1121 *Geophys. Res. Lett.*, *37*, L03,607, doi:10.1029/2009GL041482.

1122 Rella, C. (2010), Accurate greenhouse gas measurements in humid gas streams using
1123 the picarro g1301 carbon dioxide / methane / water vapor gas analyzer, *White paper*,
1124 Picarro, Inc., 480 Oakmead Pkwy, Sunnyvale, CA 94085.

1125 Sabine, C. L., et al. (2004), The oceanic sink for anthropogenic co2, *Science*, *305*(5682),
1126 367–371.

1127 Sabine, C. L., et al. (2012), Surface ocean co2 atlas (socat) gridded data products, *Earth*
1128 *Syst. Sci. Data Discuss.*, *5*, 781–804, doi:10.5194/essdd-5-781-2012.
1129 Spirig, C., et al. (2005), Eddy covariance flux measurements of biogenic vocs during echo
1130 2003 using proton transfer reaction mass spectrometry, *Atmos. Chem. Phys.*, *5*, 465–
1131 481, doi:www.atmos-chem-phys.org/acp/5/465/.
1132 Sweeney, C., E. Gloor, A. R. Jacobson, R. M. Key, G. McKinley, J. L. Sarmiento,
1133 and R. Wanninkhof (2007), Constraining global air-sea gas exchange for co2 with
1134 recent bomb 14c measurements, *Global Biogeochem. Cycles*, *21*, GB2015, doi:
1135 10.1029/2006GB002784.
1136 Takahashi, S., F. Kondo, O. Tsukamoto, Y. Ito, S. Hirayama, and H. Ishida (2005), On-
1137 board automated eddy flux measurement system over open ocean, *Sci. Online Lett.*
1138 *Atm.*, *1*, 37–40, doi:10.2151/sola.2005-11.
1139 Takahashi, T., et al. (2002), Global sea-air co2 flux based on climatological surface ocean
1140 pco2, and seasnoal biological and temperature effects, *Deep-Sea Res. II*, *49*, 1601–1622.
1141 Takahashi, T., et al. (2009), Climatological mean and decadal change in surface ocean
1142 pco2, and net sea-air co2 flux over the global oceans, *Deep-Sea Res. II*, *56*, 554–577,
1143 doi:10.1016/j.dsr2.2008.12.009.
1144 Wanninkhof, R. (1992), Relationship between wind speed and gas exchange over the
1145 ocean, *J. Geophys. Res.*, *97*(C5), 7373–7382.
1146 Wanninkhof, R., and W. R. McGillis (1999), A cubic relationship between air-sea co2
1147 exchange and wind speed, *Geophys. Res. Lett.*, *26*(13), 1889–1892.
1148 Webb, E. K., G. I. Pearman, and R. Leuning (1980), Correction of flux measurements
1149 for density effects due to heat and water vapour transfer, *Q. J. Royal Met. Soc.*, *106*,

85–100.

Weill, A., et al. (2003), Toward a better determination of turbulent air-sea fluxes from several experiments, *J. Climate*, *16*, 600–618.

Weiss, A., J. Kuss, G. Peters, and B. Schneider (2007), Evaluating transfer velocity-wind speed relationship using long-term series of direct eddy correlation co2 flux measurements, *J. Mar. Sys.*, *66*, 130–139.

Wilczak, J. M., S. P. Oncley, and S. A. Stage (2001), Sonic anemometer tilt correction algorithms, *Bound.-Layer Meteor.*, *99*, 127–150.

Yelland, M. J., B. I. Moat, P. K. Taylor, R. W. Pascal, J. Hutchings, and V. C. Cornell (1998), Wind stress measurements from the open ocean corrected for airflow distortion by the ship, *J. Phys. Ocean.*, *28*, 1511–1526.

Yelland, M. J., B. I. Moat, R. W. Pascal, and D. I. Berry (2002), Cfd model estimates of the airflow distortion over research ships and the impact on momentum flux measurements, *J. Atmos. Oceanic Technol.*, *19*, 1477–1499.

Zhang, J., X. Lee, G. Song, and S. Han (2011), Pressure correction to the long-term measurement of carbon dioxide flux, *Ag. For. Met.*, *151*, 70–77, doi: 10.1016/j.agrformet.2010.09.004.

Table 1. Recent ship-based eddy covariance CO_2 flux studies [a]

Project	Location	Season	CO_2 Methods[b]	References
GasEx-98	N Atlantic	May–June 1998	CP-IRGA	*McGillis et al.* [2001a, b]
GasEx-01	Eq. Pacific	Feb 2001	CP-IRGA	*McGillis et al.* [2004]
Arkona Spar[c]	SW Baltic	May 2003–Sept 2004	OP-IRGA	*Weiss et al.* [2007]
MR05-03	Eq. Indian	Aug 2005	OP-IRGA	*Kondo and Tsukamoto* [2007]
G.O. Sars	Greenland Sea	Jul–Aug 2006	OP-IRGA[d]	*Lauvset et al.* [2011]
Polarfront	N Atlantic	Sept 2006–Dec 2009	OP-IRGA	*Prytherch et al.* [2010a]
Knorr07	N Atlantic	May–July 2007	CP-IRGA[e]	*Miller et al.* [2009, 2010]
SO GasEx	Southern Ocn	Mar–Apr 2008	OP-IRGA	*Edson et al.* [2011]
DYNAMO	Eq. Indian	Aug 2011–Jan 2012	OP/CP-IRGA	this report
TORERO	Eq. Pacific	Jan–Feb 2012	CP-CRDS	this report

[a] Published as of October 2012

[b] CP-IRGA = closed path infrared gas analyzer (LI-COR LI6262/7000/7200); OP-IRGA = open path infrared gas analyzer (LI7500); CP-CRDS = closed path cavity ring-down infrared spectrometer (Picarro G1301)

[c] Moored spar buoy rather than ship.

[d] shrouded LI7500

[e] LI7500 converted to closed-path configuration

Table 2. DYNAMO: project median hourly F_{co_2} ($\pm 1\sigma$) for Leg 3. Flux computed as indicated in Section 3, despiked to remove extreme outliers. Results are shown for the base case (WPL and dilution corrections applied, where necessary) and for two additional water vapor cross-talk correction schemes.

		Median $F_{co_2} \pm 1\sigma$ (ppm m s^{-1})	
	Base Case	PKT [a]	Cross-correlation [b]
LI7200 lab	0.00047±0.00049 [c]	–	–
LI7200 mast	0.00663±0.00396 [d]	0.00061±0.01423	0.00122±0.00155
LI7500 mast	-0.00678±0.00314 [e]	-0.00254±0.00467	-0.00081±0.00222

[a] *Prytherch et al.* [2010b]

[b] *Edson et al.* [2011]

[c] Dry-air data – WPL and dilution correction not required.

[d] Computed from "dry" mole fraction output – should not require WPL or dilution corrections.

[e] WPL and dilution corrected.

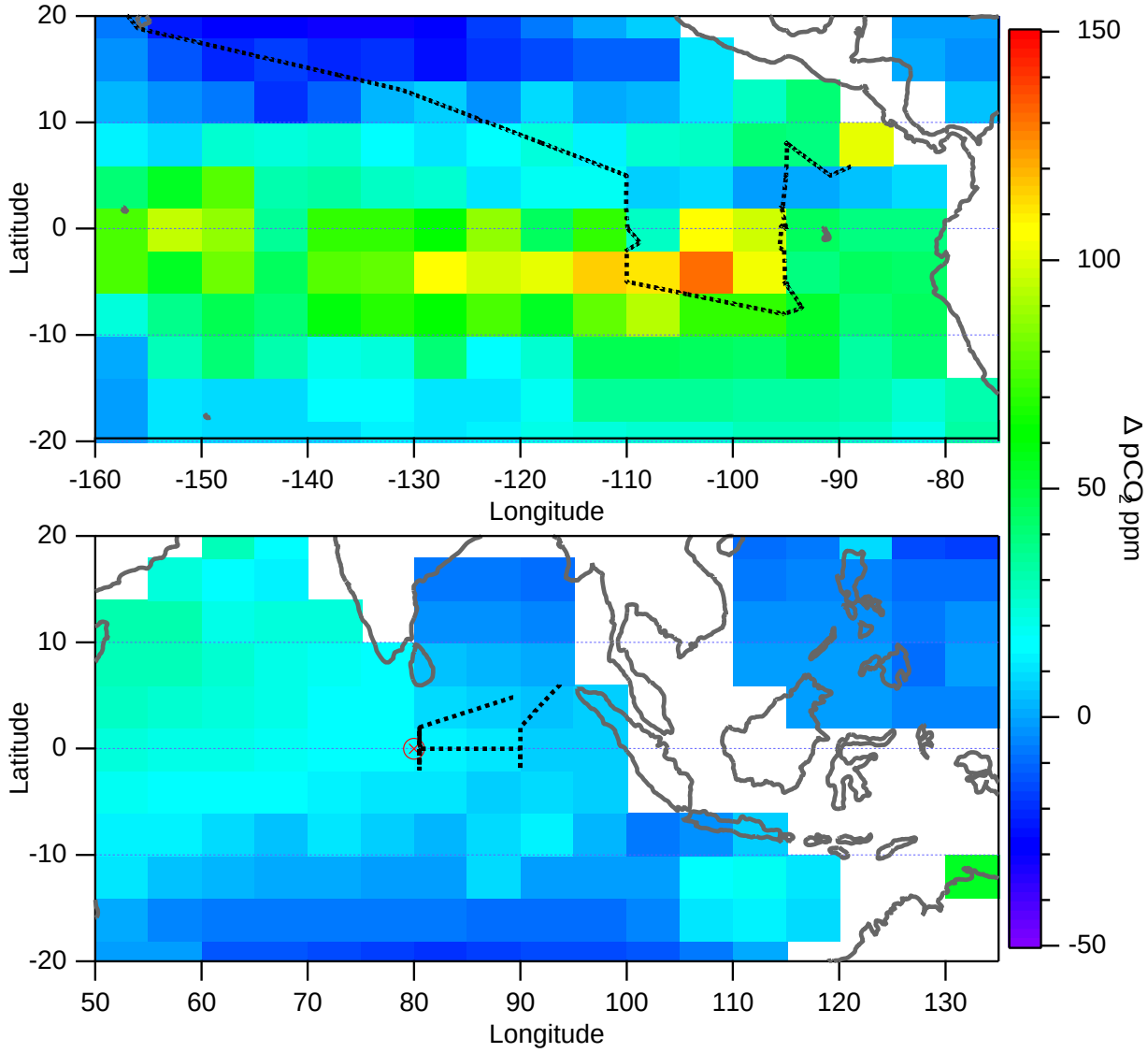

Figure 1. TORERO (Pacific Ocean) and DYNAMO (Indian Ocean) cruise tracks. ΔpCO_2 is plotted as the climatological mean for Nov–Dec (DYNAMO) and Jan–Feb (TORERO), data from *Takahashi et al.* [2009]. The DYNAMO study area is a weak source region for CO_2 with $\Delta pCO_2 \sim 30$ ppm. The TORERO cruise track transitioned from a weak sink area at 10° to 20°N into a very strong source region south of the equator in the East Pacific cold-tongue, where $\Delta pCO_2 > 100$ ppm.

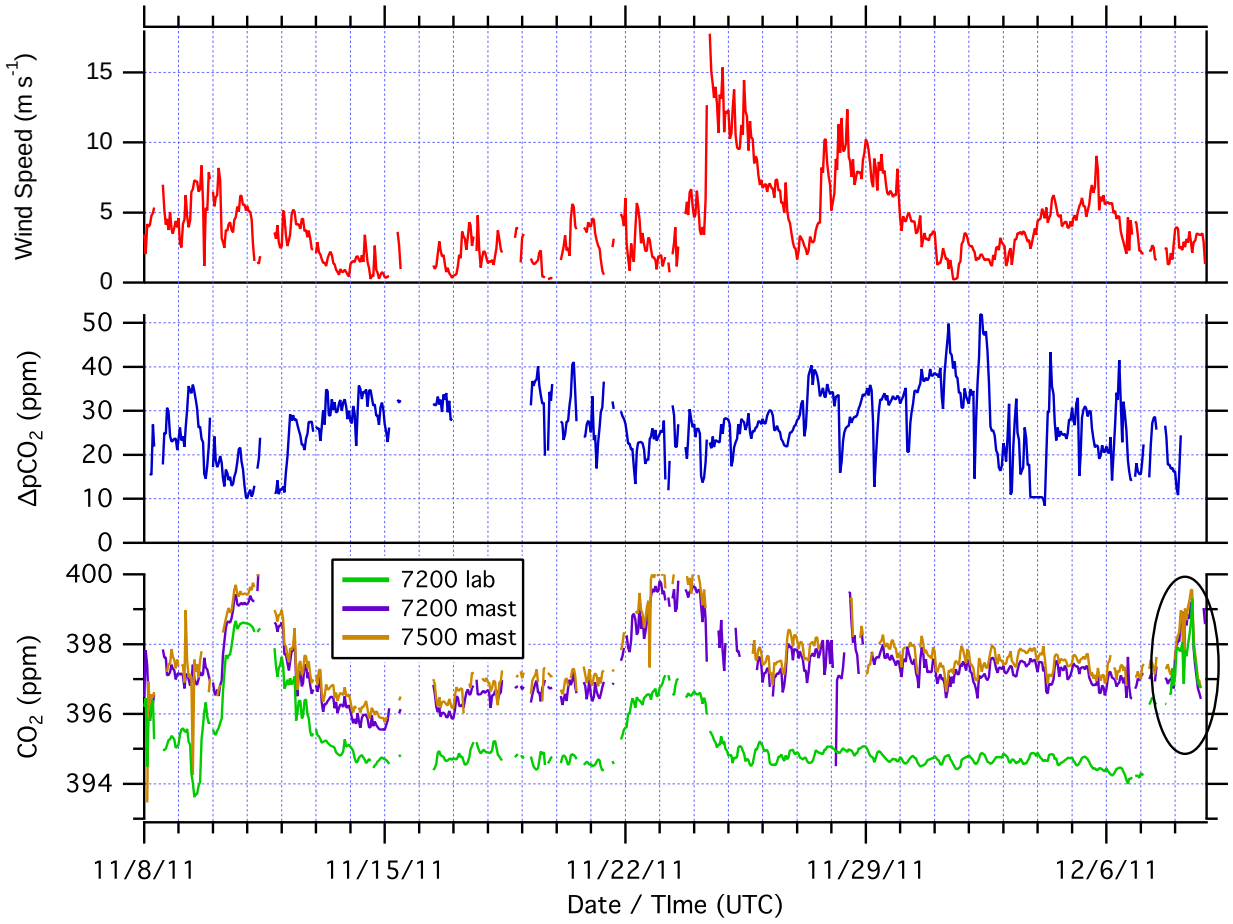

Figure 2. DYNAMO Leg 3: Time series of hourly mean wind speed, ΔpCO_2 and atmospheric dry CO_2 mixing ratio from three IRGA analyzers. An offset of 2 ppm to 3 ppm is evident between the dry-air lab LI7200 measurement and mast mounted analyzers. For the circled segment at the end of the leg, the Nafion dryer was removed from the lab LI7200 for a direct comparison with mast sensors. Without the dryer, the lab LI7200 "dry" molar mixing ratio output closely tracks the mast "dry" mole fraction measurements.

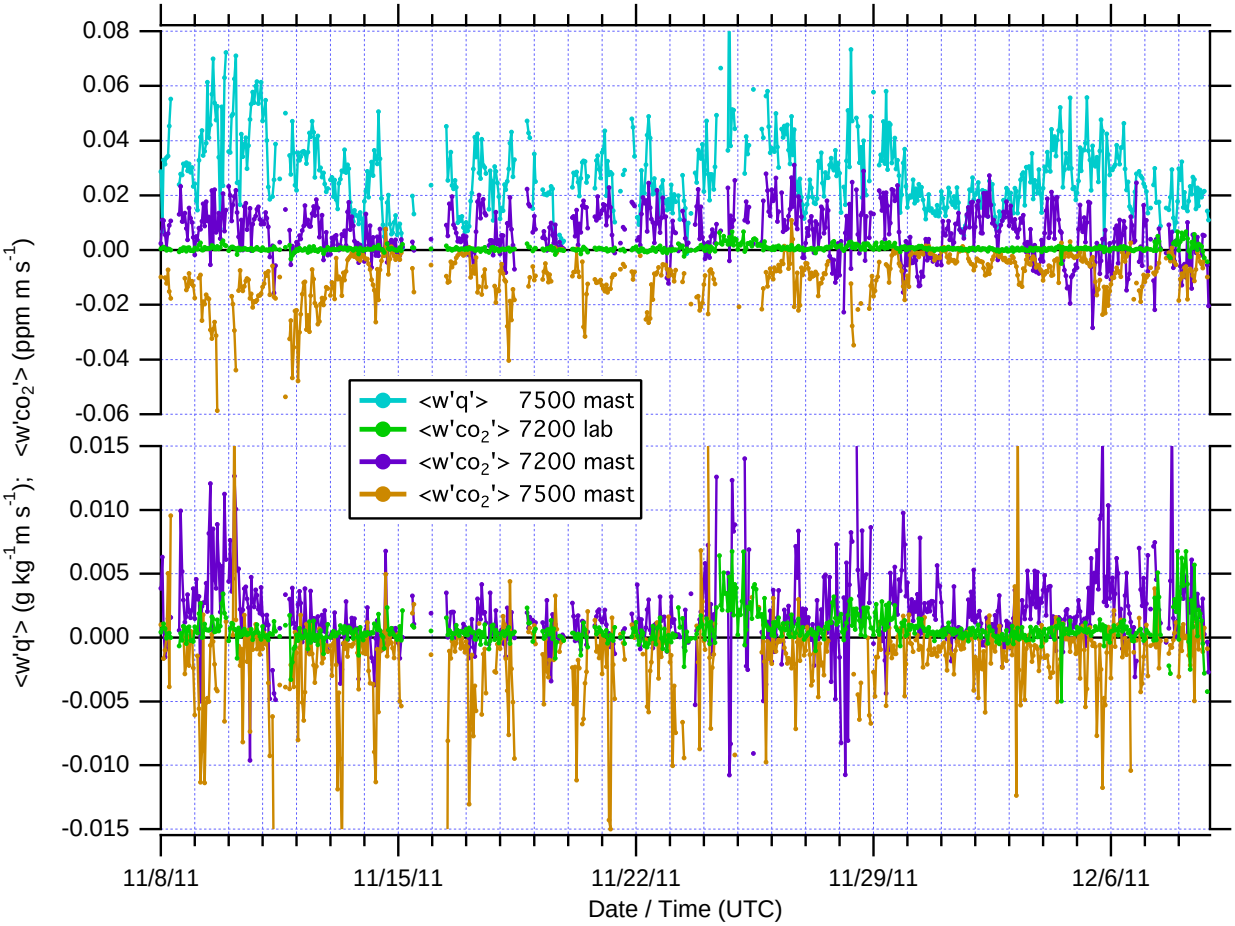

Figure 3. DYNAMO Leg 3: Time series of hourly CO_2 flux from the three IRGA analyzers. The dry-air lab LI7200 CO_2 flux is plotted in green as a reference. In the upper panel, WPL and dilution corrected CO_2 flux from mast analyzers (purple and tan traces) roughly track water vapor flux from the mast LI7500 ($\overline{w'q'}$, blue trace) and are about a factor of 14 greater than the lab LI7200 reference flux. Note, the mast LI7500 fluxes are negatively correlated to $\overline{w'q'}$ while the mast LI7200 flux correlation is positive. The lower panel illustrates application of an additional water vapor cross-correlation correction [*Edson et al.*, 2011] with $\Gamma_{7500} = 1.1$ and $\Gamma_{7200} = 0.93$ (see Section 6.2).

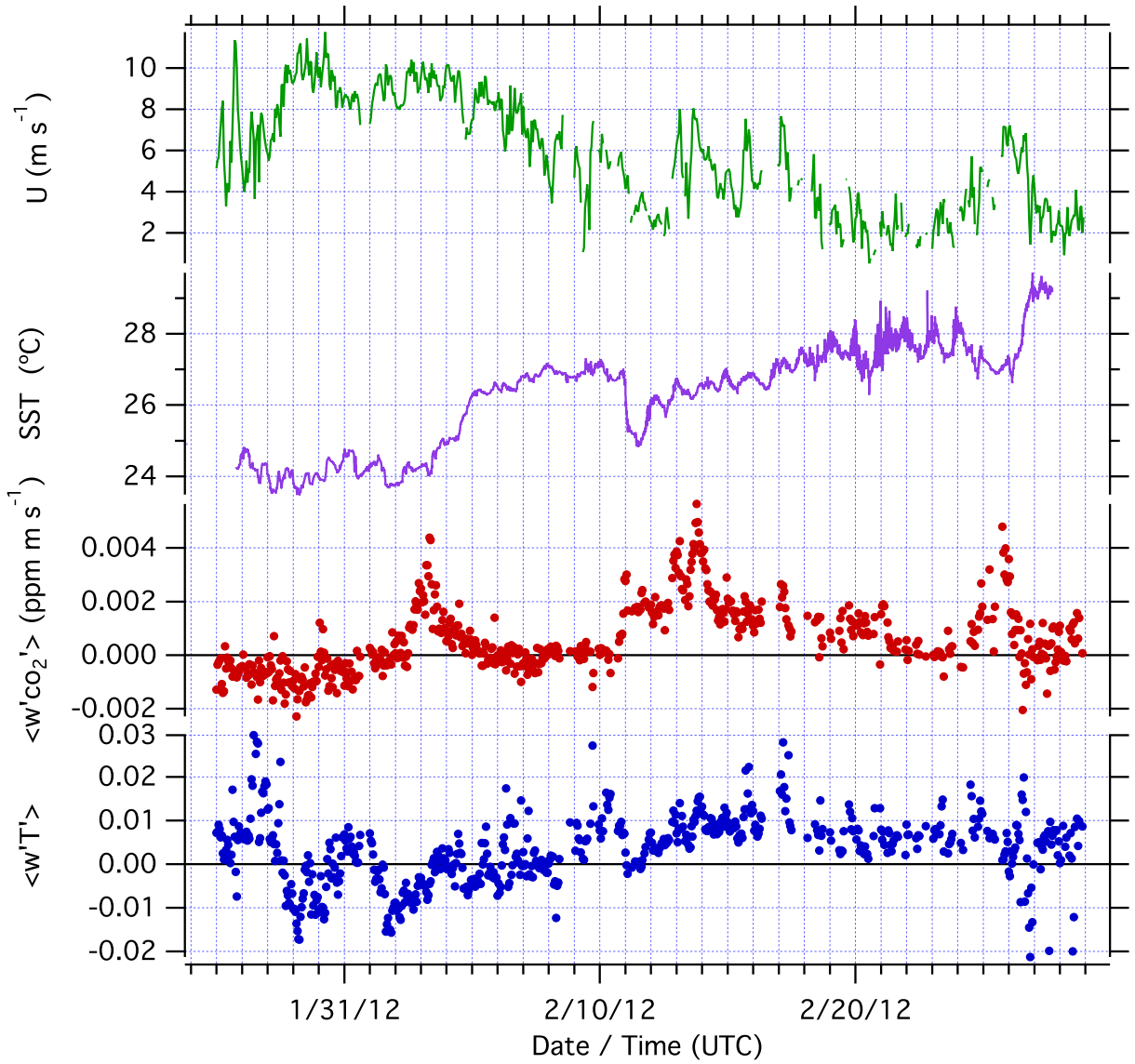

Figure 4. TORERO: hourly mean wind speed, SST, CO_2 flux and $\overline{w'T'}$. The transition to the E. Pacific cold tongue on 11-Feb is evident in the SST and CO_2 flux measurements. Prior to 11-Feb, the transition from a weak CO_2 sink region through a fairly strong, localized source region and then to equilibrium conditions (27-Jan to 10-Feb) is apparent in the flux results. For the period when flux is near zero (5- to 10-Feb) $\sigma_{F_{co_2}} = 2.4 \times 10^{-4}$ ppm m/s. $\overline{w'T'}$ was generally less than $0.01\,^{\circ}\mathrm{C\,m\,s^{-1}}$ throughout.

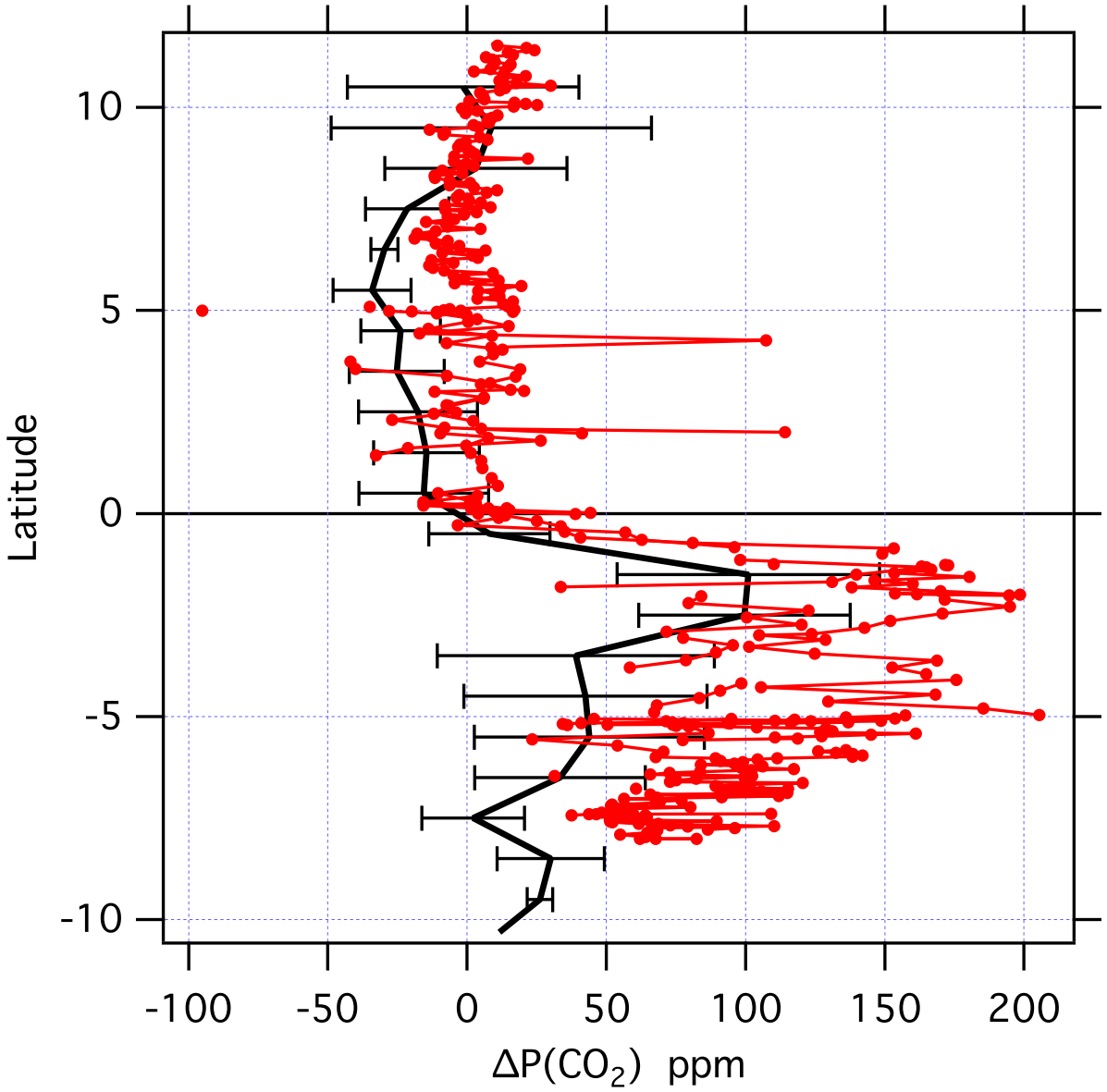

Figure 5. TORERO: ΔpCO_2 in the equatorial region of 95 °W and 110 °W. Red trace: estimated from observed F_{co_2} and computed k_{co_2} (COAREG 3.0). Blue trace: Jan-Feb mean for cruises along 95 °W and 110 °W from the gridded SOCAT database [*Sabine et al.*, 2012]. Error bars are 1σ.

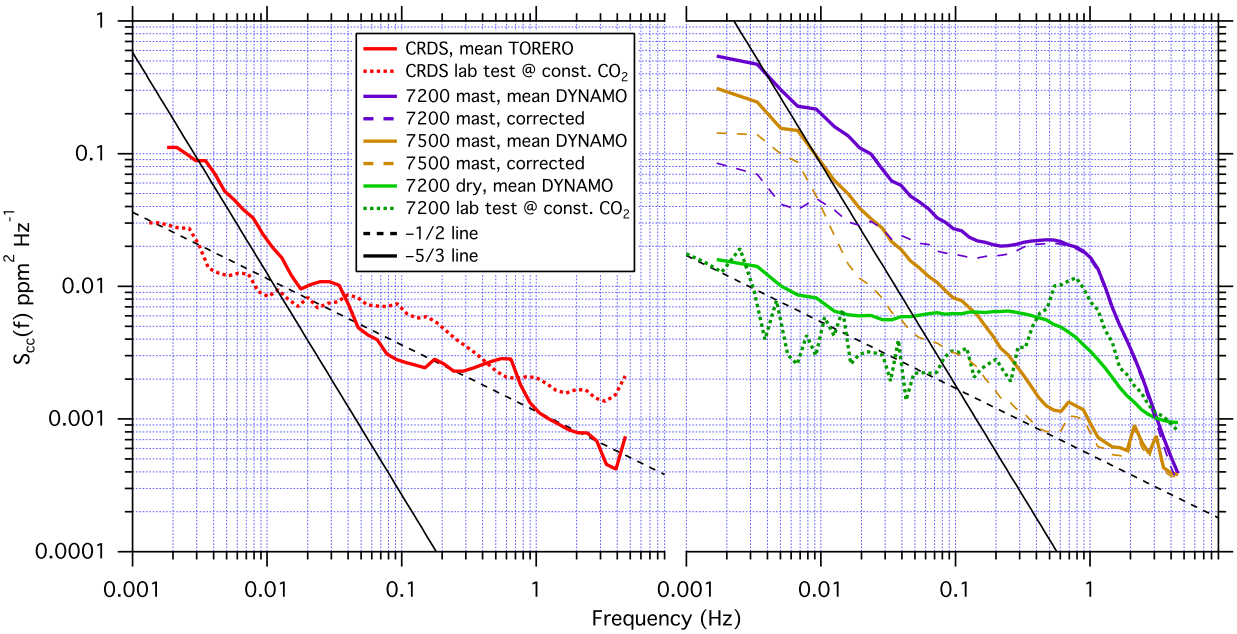

Figure 6. Mean variance spectra for the CO_2 analyzers. Lab tests at constant CO_2 are shown as dotted lines. Left panel: CRDS spectra showing a characteristic "pink" noise background with a slope of $\sim -1/2$. The TORERO spectrum shows some indication of a -5/3 turbulence relationship at low frequencies, but is otherwise dominated by analyzer noise. Right panel: IRGA spectra from DYNAMO, which also show a "pink" background noise characteristic. Application of the cross-correlation correction for water vapor interference [*Edson et al.*, 2011] is shown as dashed lines. LI7200 spectra exhibit a broad hump of unknown origin peaking near 0.3 Hz to 0.6 Hz. A similar feature is noted in the raw LI7200 absorbance data for dry air DYNAMO measurements and in the lab test (dotted green), so the effect is not related to water crosstalk or motion.

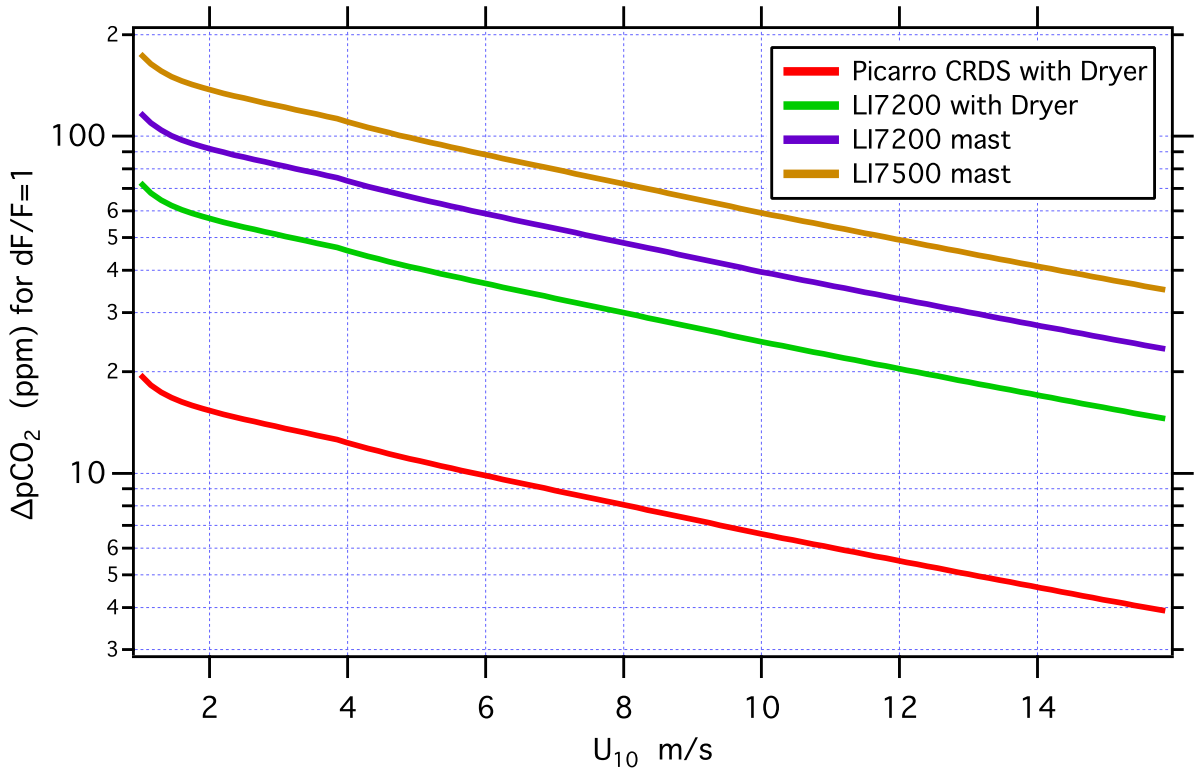

Figure 7. Flux detection limit criterion versus wind speed for each analyzer, expressed as $\Delta p\mathrm{CO}_2$ ppm necessary for $\delta F/F$ =1 (i.e. 100 % error in observed F_{co_2} over 1 hr sampling time) under slightly unstable, stationary conditions. These results assume effective removal of water vapor cross talk bias in LI7500 and LI7200 analyzers (see Section 6.2).

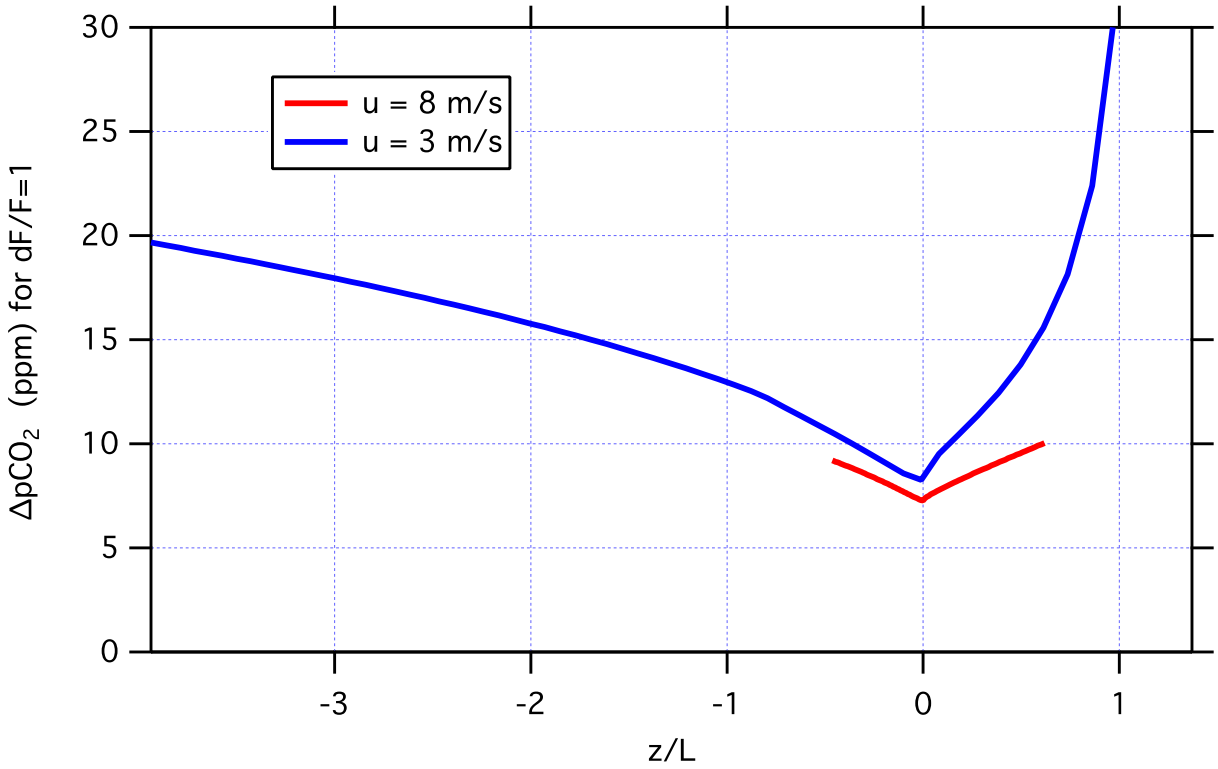

Figure 8. Flux detection limit criterion for the CRDS analyzer versus stability parameter z/L, given as $\Delta p\mathrm{CO}_2$ ppm for $\delta F/F$ =1 (100% error in observed F_{co_2} for 1 hr sampling time) under stationary conditions at low and moderate wind speeds. $\Delta p\mathrm{CO}_2$ computed from Equation (9). z/L and u_* obtained from the COARE 3.0 bulk flux model for two wind speeds with all input variables except air temperature held constant: T(air) = 8 °C to 16 °C, SST = 12 °C, RH = 80%, and u= 3 m s^{-1} or 8 m s^{-1}. Flux detection limit increases rapidly for stable conditions ($z/L > 0.5$) and light winds.

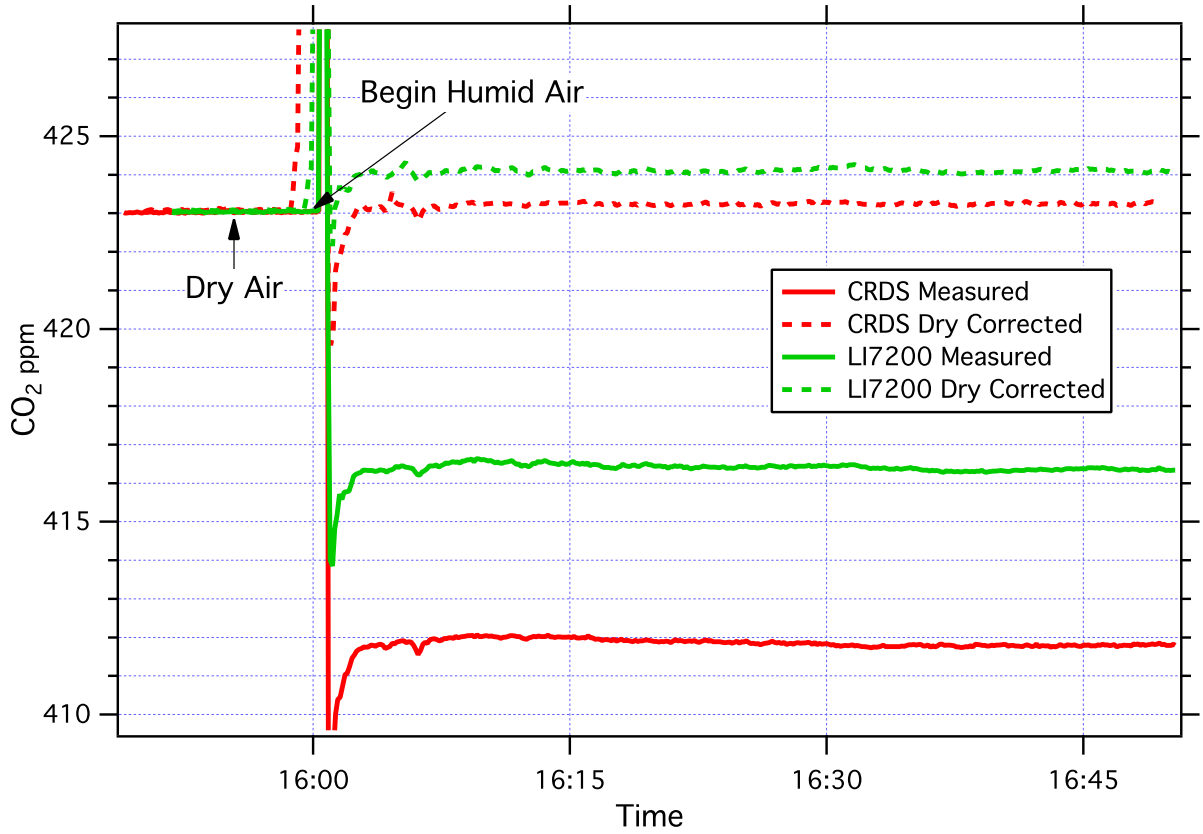

Figure 9. Laboratory test of CO_2–H_2O cross-sensitivity. Ten-second average data in dry air from a compressed gas cylinder. At 16:00, dry air flow was diverted through a Nafion humidifier, increasing dew point to ∼15 °C, or ∼11 g kg^{-1} specific humidity. The observed CRDS concentration, uncorrected for either line broadening or dilution, decreases by more than 10 ppm (red trace). The LI7200 wet mole fraction output, corrected for band broadening in the analyzer but not for dilution, decreases by 6.5 ppm (green trace). Application of the manufacturer's recommended corrections for the CRDS [*Rella*, 2010] results in a slight over correction of ∼ 0.1 ppm (red dashed). The sum of dilution and band broadening corrections for the LI7200 yields a 1.1 ppm overcorrection compared to the dry-air value. (green dashed).

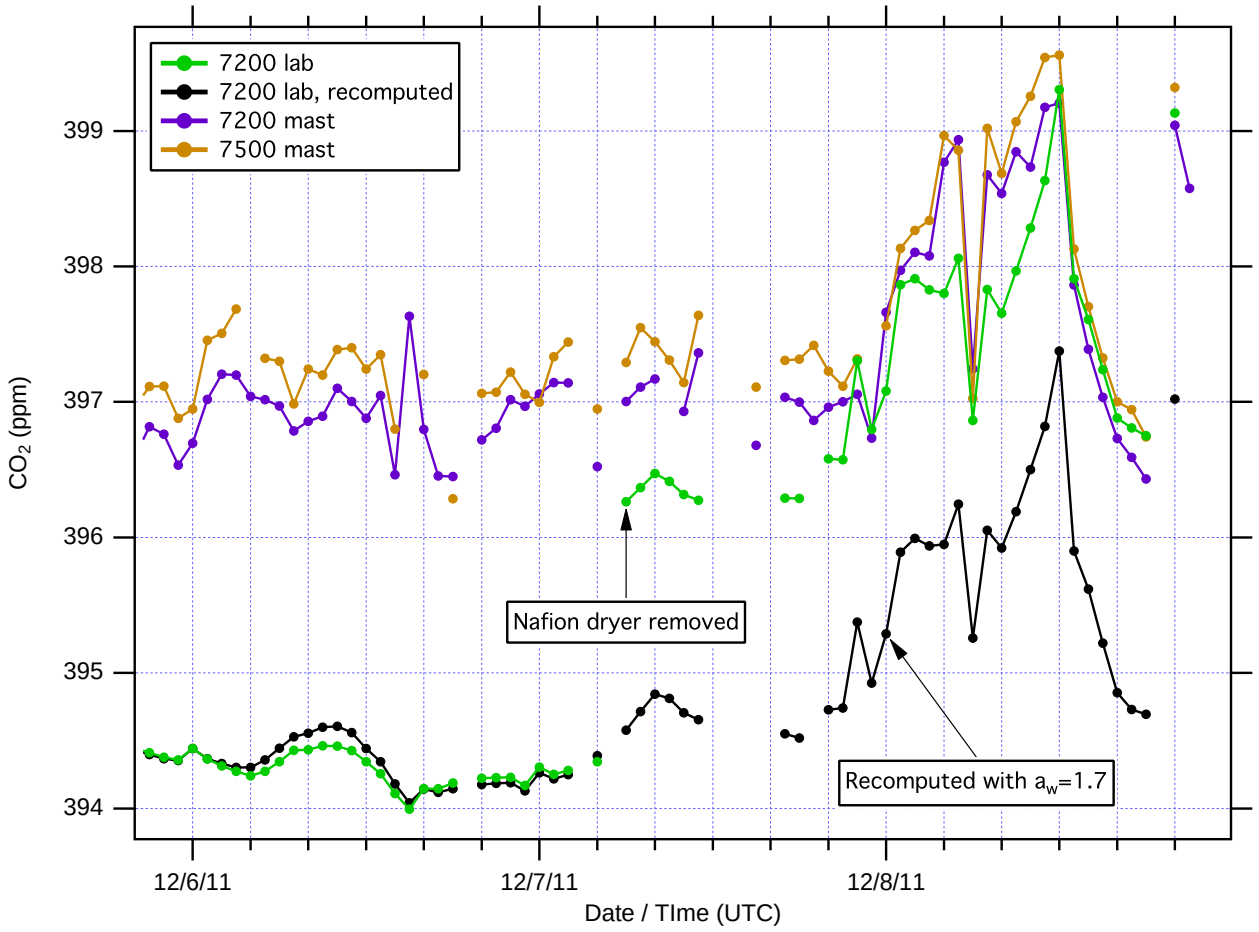

Figure 10. DYNAMO: CO_2 measurements for 6-Dec through 8-Dec. After 0400 UTC on 7-Dec, the Nafion air dryer was removed from the lab LI7200. From that point on, the dry mole fraction output of the lab LI7200 closely tracks dry mole fraction from the two mast-mounted IRGA analyzers. Recomputing the lab LI7200 dry molar mixing ratio from raw absorbances (black trace) with an adjusted water crosstalk constant (a_w = 1.7 rather than 1.15) closely matches the analyzer-computed result for the period with the dryer and does not show a bias following removal of the dryer. Adjusting the cross-sensitivity factor, X_i, produces a similar effect.

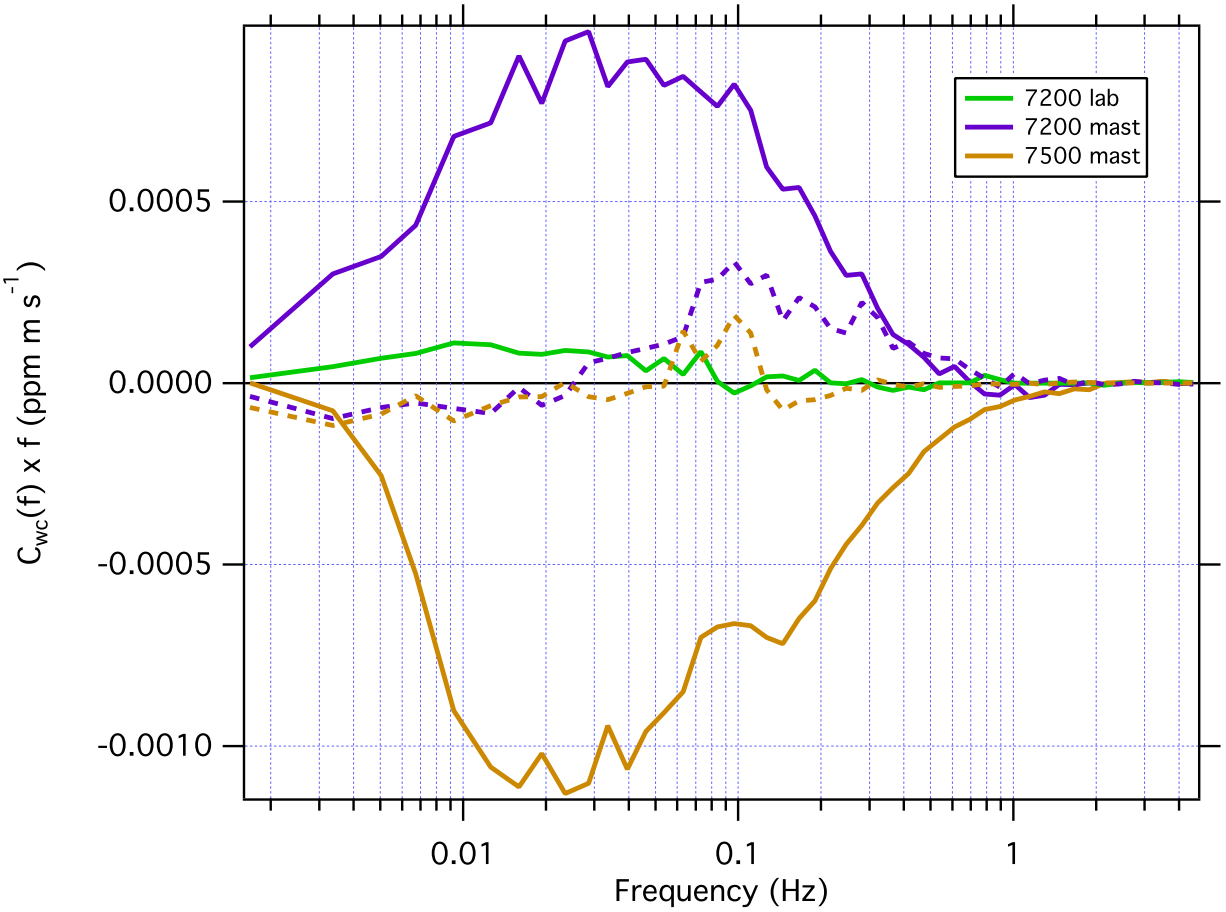

Figure 11. DYNAMO: Project mean cospectra for the IRGA analyzers. Application of the cross-correlation correction for water vapor crosstalk as described in the text (dashed lines) brings the mast IRGA cospectra closer to the dry-air LI7200 result. Spectral shape is distorted but fluxes are also very small.

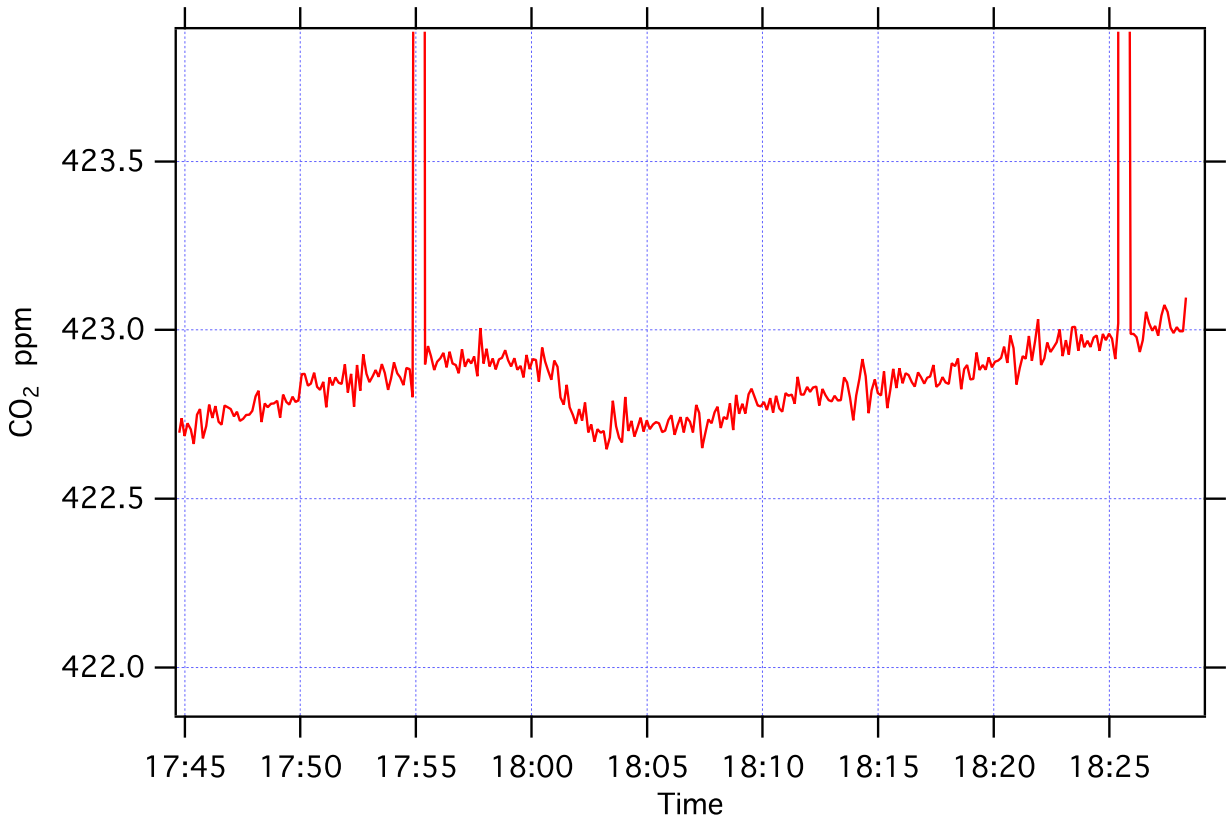

Figure 12. Laboratory test of CRDS water vapor sensitivity with a 200-tube Nafion dryer. Ten-second average data in dry air from a compressed gas cylinder. At 17:55 humidity is increased to $\sim$11 g kg^{-1} and at 18:25 dry air flow resumes. Other than a slow drift of $\sim$0.3 ppm, no abrupt shift in response is apparent for a very large change in input water vapor. Dew point at the dryer output is <-10 °C throughout. In this case, concentration drift is due to incomplete temperature and pressure equilibration of the CRDS cavity.

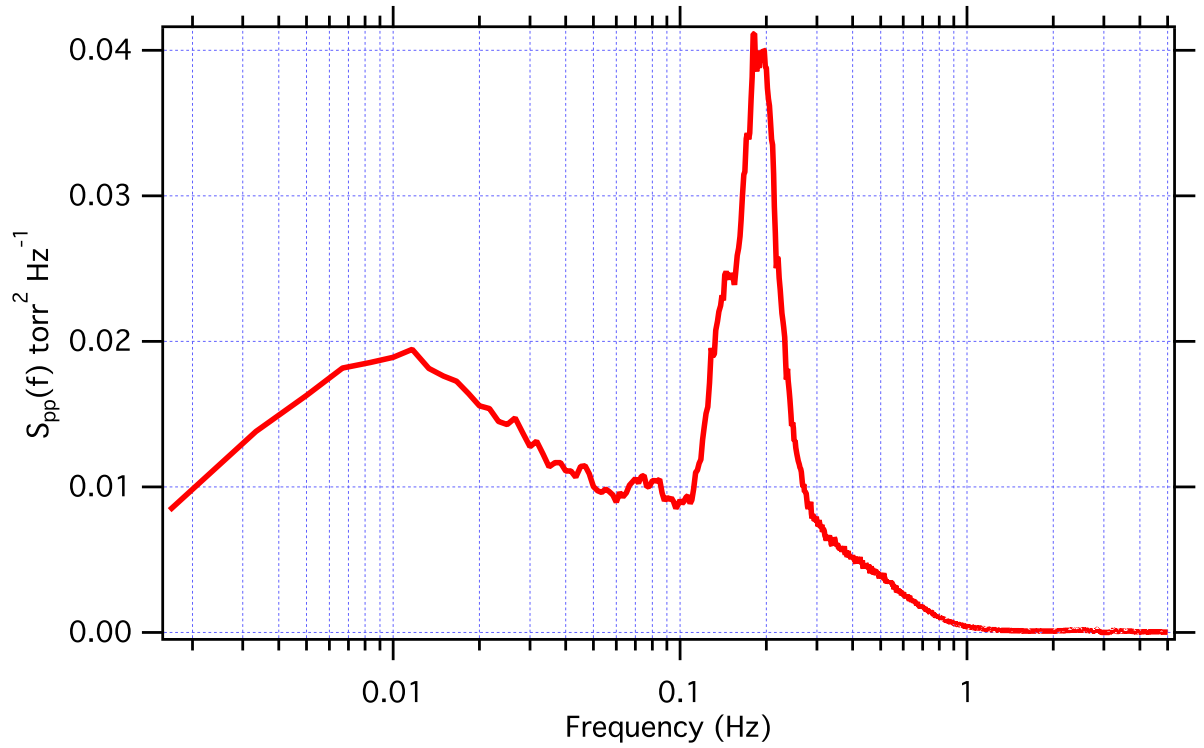

Figure 13. Mean CRDS cavity pressure spectrum for the first 100 hours of the TORERO cruise, when ship motion was greatest. Motion sensitivity of the pressure control system is apparent in the peak at 0.2 Hz.

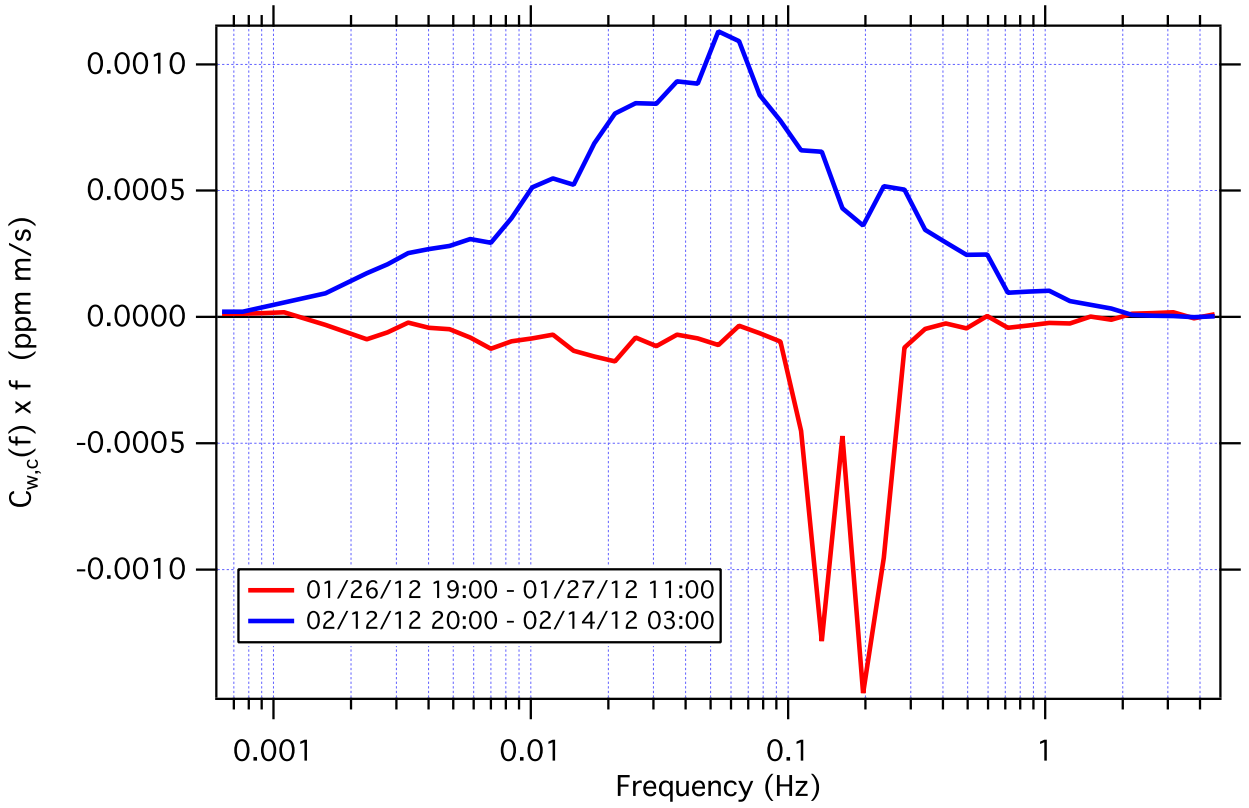

Figure 14. TORERO: CRDS cospectra for a 16-hour period early in the cruise with low negative F_{co_2} and high ship motion (red trace) and a 7-hour period of high positive F_{co_2} and low ship motion (blue trace). The motion effect is evident at 0.1 Hz to 0.3 Hz in the red trace. For the few measurements most affected by motion, a corrected estimate of the flux was obtained by fitting a baseline under the cospectral motion peak and removing it from the flux computation.

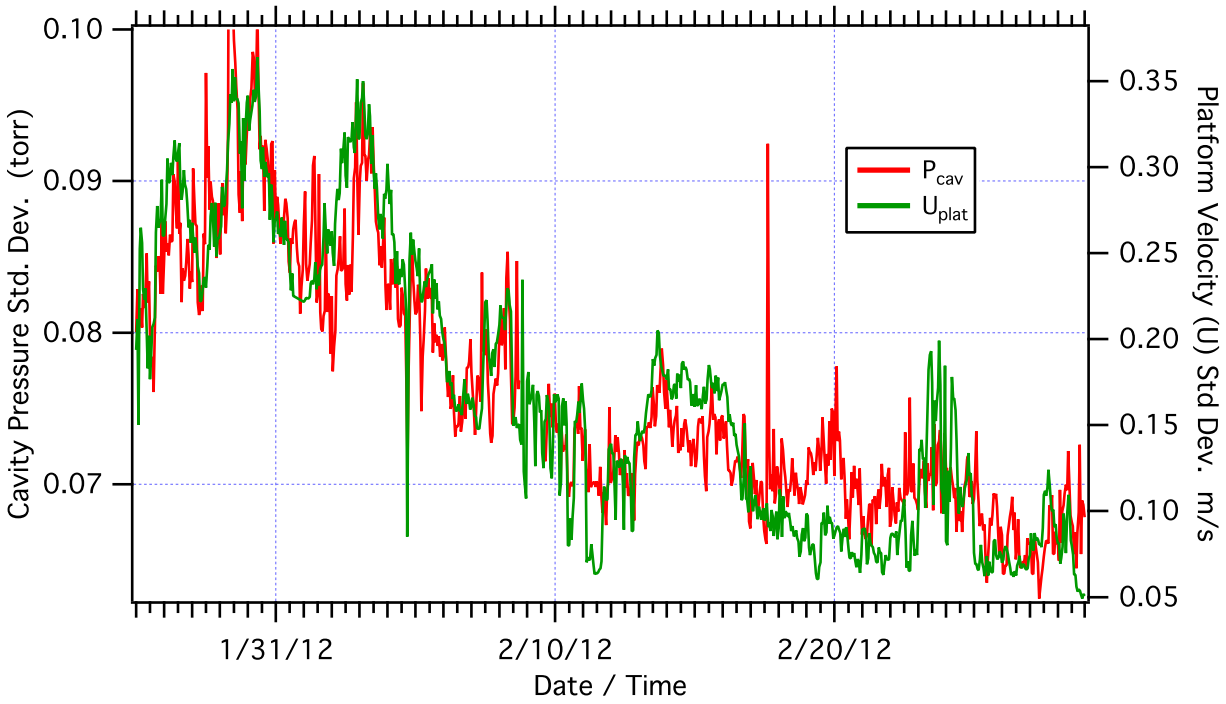

Figure 15. TORERO: Standard deviation in CRDS cavity pressure (red trace) and fore-aft platform velocity, U_{plat} (green trace).

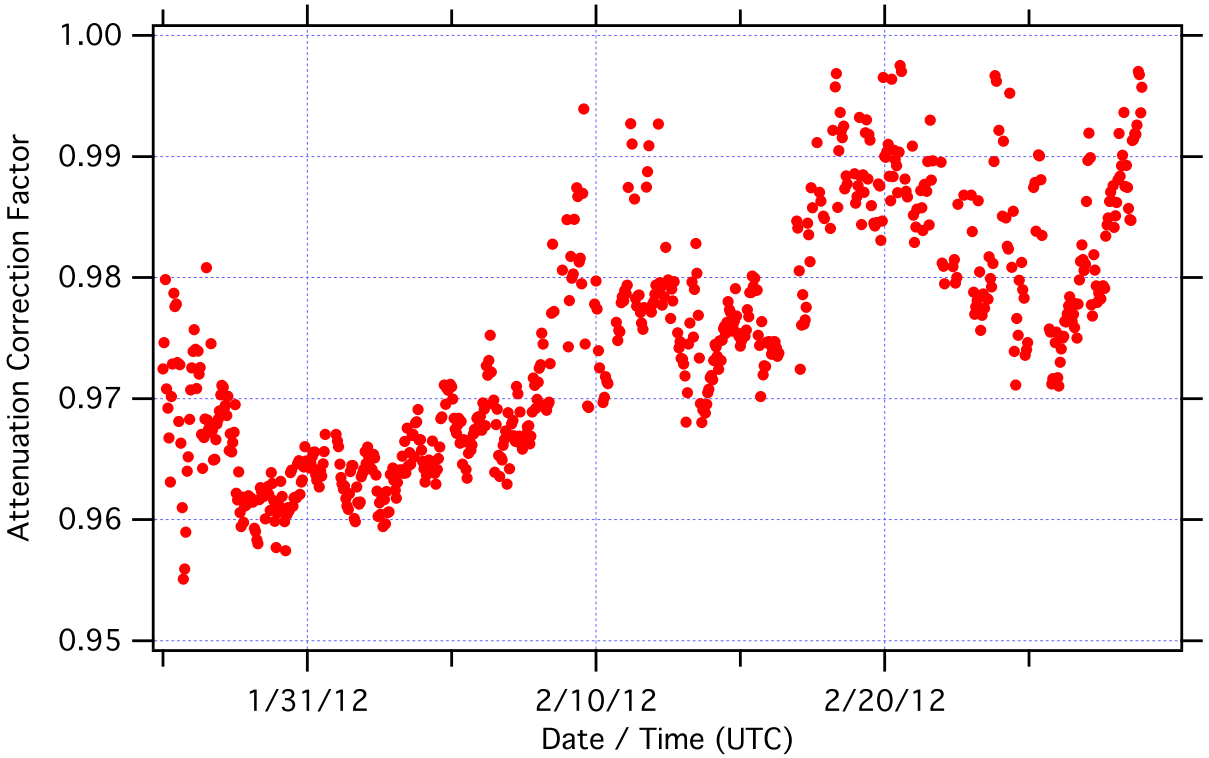

Figure 16. TORERO: Hourly frequency attenuation correction factors computed from the step impulse response to hourly 3-second synchronization "puffs". Observed flux is divided by the attenuation correction factor to account for the low-pass filtering effects of the inlet tubing, air dryer and analyzer cavity volume. The correction is less than 4 % in almost all cases.

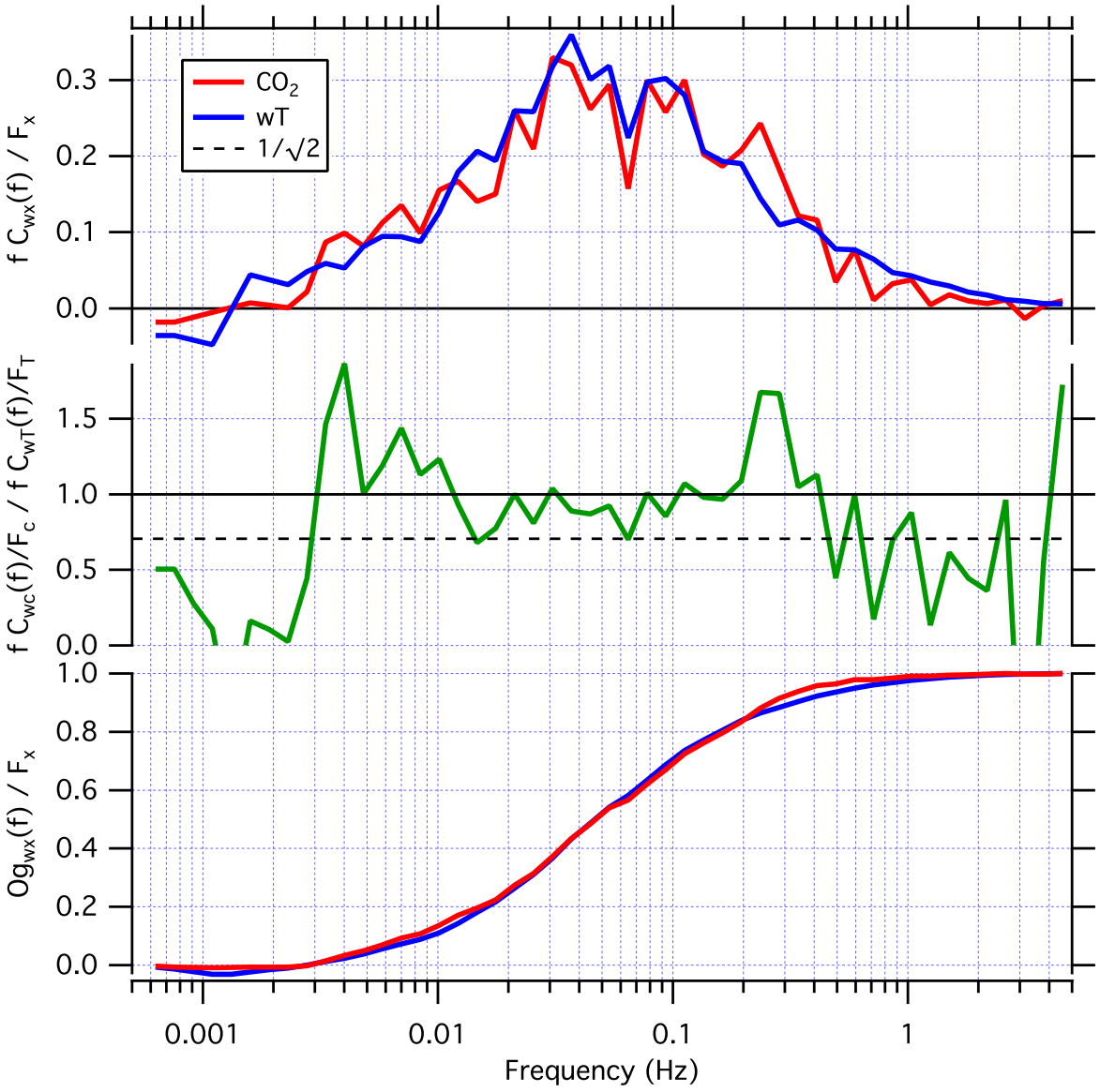

Figure 17. TORERO: Normalized $\overline{w'co_2'}$ and $\overline{w'T'}$ cospectra, cospectral ratio (green trace) and Ogives for 15-Feb, 1600–2300 UTC. This period is characterized by fairly large CO_2 and sensible heat fluxes with moderate winds ($\overline{u}_r = 9.3\,\mathrm{m\,s^{-1}}$, $\overline{u}_{true} = 6.2\,\mathrm{m\,s^{-1}}$). Nevertheless, noise prevents a clear determination of f_c from the cospectral ratio – the point where the ratio drops by $1/\sqrt{2}$, shown by the dotted line. Normalized Ogives for this period are identical within the precision of the data, confirming a small attenuation correction. Ogive curves approach the low frequency asymptote smoothly, indicating 30 minute integrations have adequately captured low frequency flux signal.

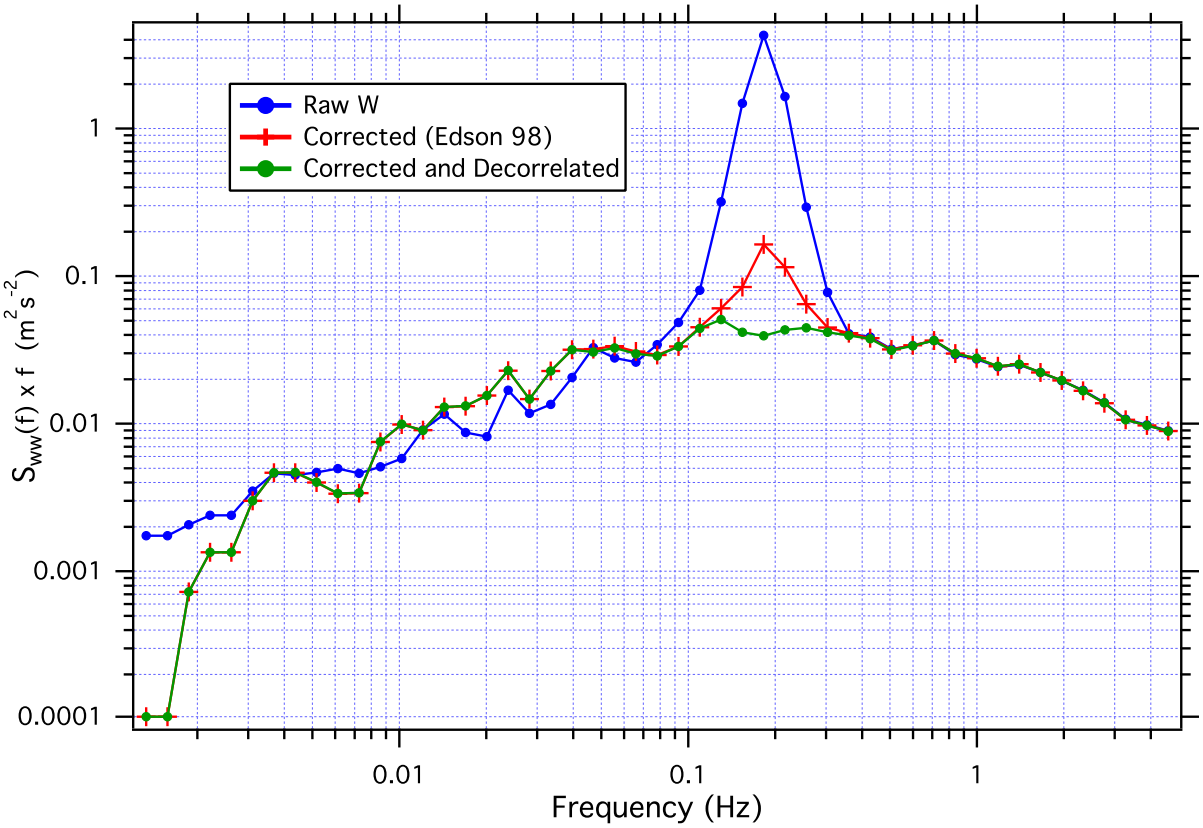

Figure 18. TORERO: w spectra for 30-Jan-2012 0900 UTC – a period of significant ship motion, illustrated by the large peak at ∼0.2 Hz in the raw w spectrum (blue trace). Motion correction per *Edson et al.* [1998] yields the red trace. Further correction through decorrelation of w and platform vertical acceleration and velocity (green trace) removes residual motion contamination.

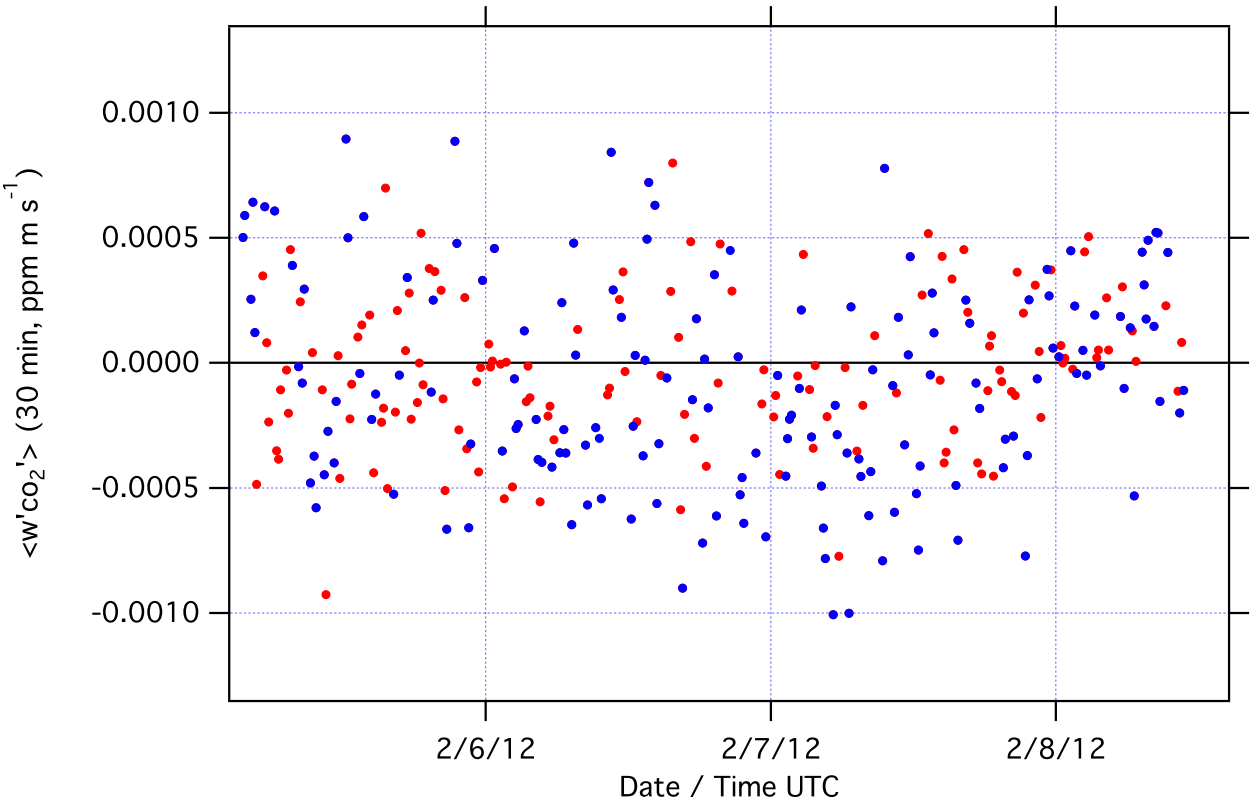

Figure 19. TORERO: CO_2 flux measurements from 5-Feb to 8-Feb-2012 (T =30 min), when measurements were uniformly distributed about zero. The covariance ratio stationarity test [*Foken and Wichura*, 1996] eliminates red data points. These observations are retained by alternate stationarity criteria illustrated in Figure 20.

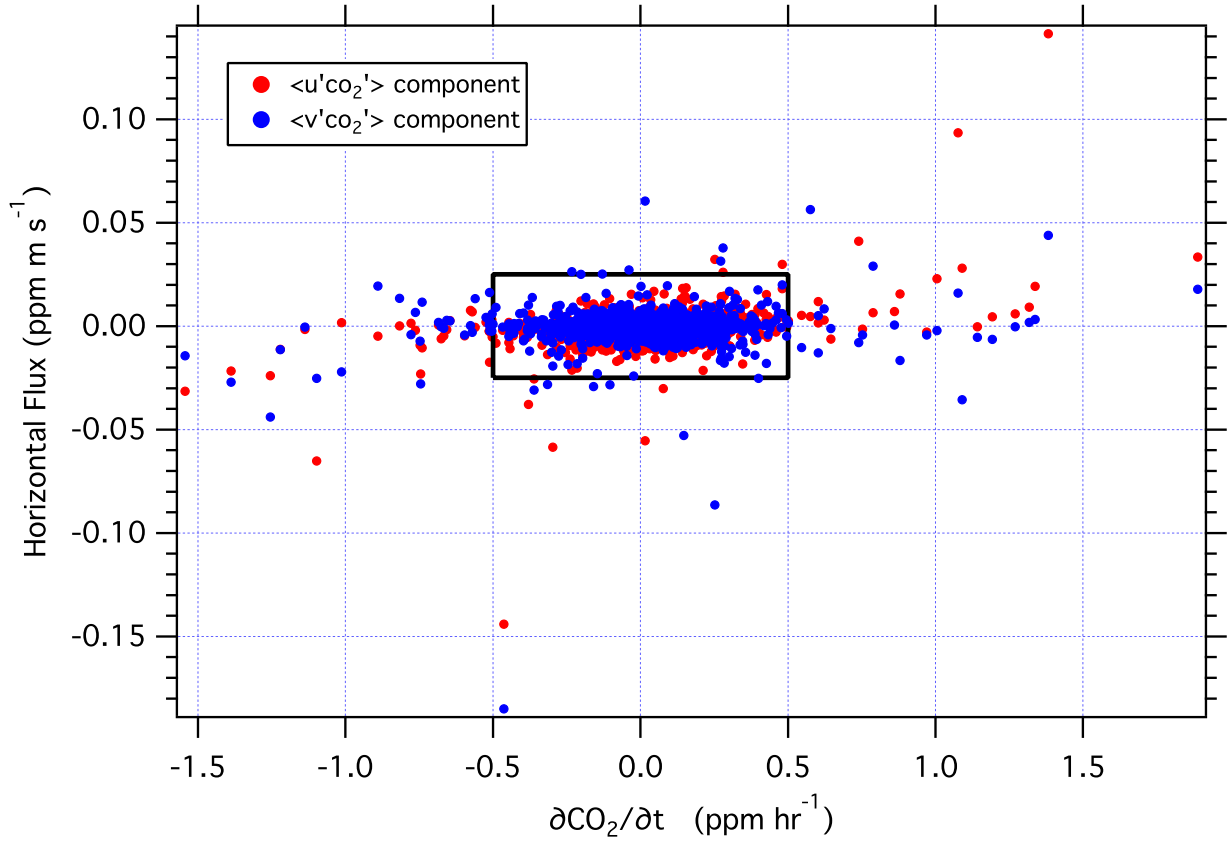

Figure 20. TORERO CO_2 steady-state criteria: $\overline{v'co_2'}$ (blue) and $\overline{u'co_2'}$ (red) turbulent fluxes versus $\partial CO_2/\partial t$ for 30-minute data segments. Flux measurements corresponding to points outside the black bounding box are excluded from the final hourly mean flux values. Note, limits to the magnitude of horizontal turbulent flux reflected by the bounding box are quite large (10x) compared to the range of vertical turbulent flux in Figures 4 or 21.

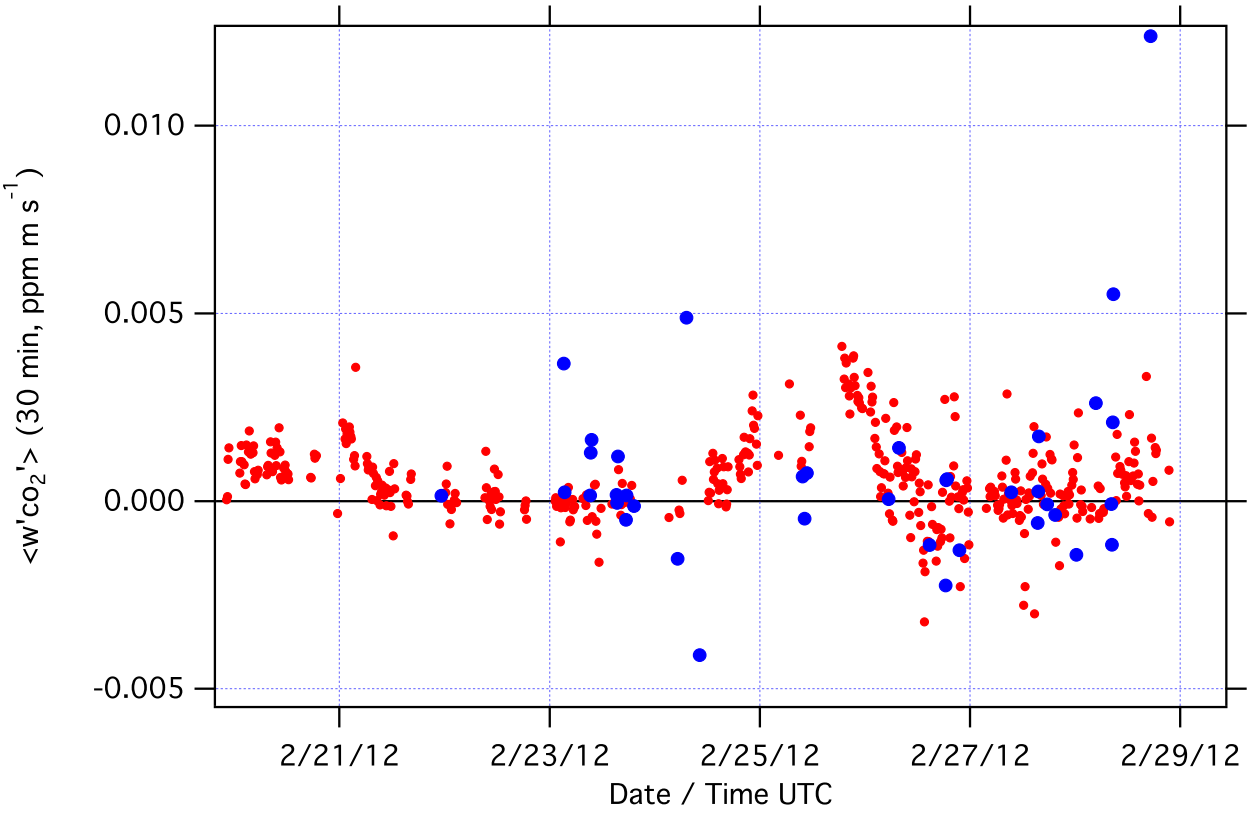

Figure 21. TORERO: CO_2 flux segment from late in the cruise illustrating instances where measurements were discarded (blue dots) on the basis of stationarity criteria in Figure 20.